

REVIEWS OF TOPICAL PROBLEMS

PACS numbers: **87.10. – e**, 87.16.Nn, 87.19.L –

Energetics and stochastic dynamics of intraneuron transport

Yu M Romanovsky, V P Trifonenkov

DOI: 10.3367/UFNe.0186.201602b.0125

Contents

Abstract. Walking molecular motors performing various functions in living cells are reviewed, including kinesin, myosin V, and dynein. These motors ensure the transport of neuromediators in neurons and are therefore crucial for interaction among the hundred billion brain cells. Functional schemes based on these motors are presented, and corresponding mathematical models are constructed as systems of two coupled FitzHugh–Nagumo equations. However, polynomials describing the moments of force are of high order and nearly N-shaped. Model parameters are determined from motor functional schemes that are based on observed data from X-ray structural analysis, cryogenic electron microscopy, laser tweezer measurements, and fast point marker-based videomicroscopy. Basic data on neuron energetics are summarized.

Keywords: neuron, molecular motors, kinesin, myosin V, dynein, adenosine triphosphate (ATP), active site

Yu M Romanovsky Lomonosov Moscow State University,
Faculty of Physics,
Leninskie gory 1, str. 2, 119991 Moscow, Russian Federation
E-mail: yuromanovsky@yandex.ru
V P Trifonenkov National Research Nuclear University "MEPhI",
Kashirskoe shosse 31, 115409 Moscow, Russian Federation

Received 12 October 2015, revised 11 November 2015
Uspekhi Fizicheskikh Nauk **186** (2) 125 – 145 (2016)
DOI: 10.3367/UFNr.0186.201602b.0125
Translated by Yu V Morozov; edited by A Radzig

> *Are we in a position to say*: *Give me matter and I will show you how a caterpillar can be created*? *Do we not get stuck at the first step due to ignorance about the true inner nature of the object and the complexity of the diversity contained in it*? *It should therefore not be thought strange if I dare to say that we will understand the formation of all the heavenly bodies, the cause of their motion, in short, the origin of the whole present constitution of the Universe sooner than the creation of a single plant or caterpillar becomes clearly and completely known on mechanical grounds.*
>
> *Universal Natural History and Theory of Heaven*, I Kant

1. Introduction

In recent decades, the processes by which the Universe formed and evolves have been the focus of attention of astrophysicists armed now not only with increasingly sophisticated observation techniques but also with a detailed theory making use of mathematical models. The same is the case with human brain research. The complexity and unique capabilities of the brain

provide a basis for elaborating a model of the Universe itself. In this sense, the human brain is the pinnacle of matter development and organization. Certainly, Immanuel Kant was right when he stated that mechanics alone is not enough to comprehend the constitution and functions of living organisms, to say nothing of their nervous system.

1.1 General information on the human brain

There are about 100 billion neurons in the human brain and almost as many glial cells located between them and separating neurons from blood vessels. To recall, the number of glial cells in the human brain may increase several-fold through time. They supply the neurons with glucose and metabolic substrates, and regulate ion concentration in the extracellular space and local blood flow. The glial cells can coordinate the work of synapses of neurons that are not connected directly with one another.

It can be said that brain structures (cerebral cortex, cerebellum, medulla oblongata, etc.) are actually highly organized intercommunicating colonies of neurons. These neurons also communicate with one another inside the colonies and are connected through the ramified axonal network with sense organs, muscle cells, etc.

It should be noted that glia most probably plays an important role in information processing in the brain as well. Excitation waves propagating in the glia cannot be regarded as belonging to a single class of waves, since they exhibit different properties depending on the heart rate and neuron excitation pulses; in other words, their collisions lead to annihilation, interference, and passage through one another.

Generally speaking, the cognitive process depends on the events taking place in both glial cells and neural networks of the brain (see materials of the *Fifth Congress of Russian Biophysicists* held in 2015, e.g., paper [1]). The description of these extremely complicated processes is beyond the scope of the present review, which focuses on a simpler problem formulated in its title. Molecular motor (MM)[1]-related issues were also widely discussed at the *Fifth Congress*.

Neurons are from 5 to 120 (mean 10–30) μm in size. The largest nerve cells in the human body are spinal motoneurons and giant Betz pyramids of the cerebral cortex. Both are actually motofacient cells, and their branching is needed to accommodate a large number of axons and dendrites from other neurons. There are roughly 10,000 synapses per neuron in the cortex.

Neurons interact with one another and with target cells through the agency of neuromediators; they are conditionally classified into two groups: excitatory and inhibitory. Two neurons are physically connected through synapses, i.e., junctions formed between one neuron's axon terminals and the other's dendrites, axons, or body. An excited neuron therewith releases the neuromediator into the synaptic cleft and acts on membrane receptors of the 'attacked' neuron. Each neuron produces its specific mediator, which is admitted by receptor channels of the partner neuron. Gamma-aminobutyric acid (GABA) is the most widespread inhibitory neuromediator, and glutamic acid (glutamate) is the most common excitatory or initiating neuromediator.

1.2 Molecular motors in the service of neurons

The objective of the present review — extending the previous one [2] devoted to the nano-sized motor/generator F_0F_1-ATPase — is to describe the stochastic dynamics of MMs supporting intraneuronal transport, viz. kinesin, myosin V, and dynein. It is these MMs that are responsible, together with acetylcholinesterase (molecular 'scissors'), for the turnover of neuromediators and waste molecules in synaptic contacts between different neurons, as well as between neurons and other target cells.

The 'protein machine' concept is now perfectly elaborated (see, for instance, Refs [3, 4]). Even before the structure of rotary ATPase motor/generators and walking MMs became known, the authors of the concept had been well aware that each cycle of an enzyme-driven reaction was related to internal movements of individual molecular groups that not only altered the configuration of electric fields in the 'pockets' of active centers (ACs) but also accumulated and stored potential energy in enzyme-forming subglobules.

The pioneers of MM research, Paul Boyer (USA) and John Walker (UK), shared the Nobel Prize in Chemistry 1997,[2] awarded for "their elucidation of the enzymatic mechanism underlying the synthesis of adenosine triphosphate (ATP)," with Jens Skou (Denmark), who received the award "for the first discovery of an ion-transporting enzyme, Na^+, K^+-ATPase."

A detailed description of the rotary F_0F_1-ATPase motor can be found in Refs [2, 5]. As concerns the Na^+, K^+-ATPase molecular pump maintaining, in particular, membrane potentials (not only in neurons), its functional design is known fairly well, but elaboration of its mathematical models remains to be completed.

The main ideas and principles behind ATPase operation find application in the models of walking MMs, such as kinesin, myosin V, and dynein. It is significant that actomyosin interactions were well investigated in muscle cell sarcomeres (see review [6]), while dyneinic motors in complexes maintaining the mobility of flagella [7]. On the other hand, walking MM studies began only recently. Kinesin was discovered in 1984 by Ronald D Vale, affiliated with University of California, San Francisco, USA [8, 9].

Microtubules (MTs) composed of tubulin serve as tracks for MMs moving from cell nucleus to synaptic terminals, where the transporter, myosin V, walks over an actin filament (AF) network.

Let us discuss, before dealing with the kinesin, myosin V, and dynein structure and function, the cargoes they are known to carry. These are, first and foremost, vesicles containing neuromediator molecules. They are continually delivered to synapses to attach near the synaptic terminal membrane. When a nervous impulse excites the membrane, the vesicle contents are ejected into the synaptic cleft. A neuromediator, e.g., acetylcholine, reaches receptors on the target cell, making them stimulate generation of a nervous impulse inside it or, for example, release Ca^{2+} ions stored in muscle cells. This is one of the most important forms of neuron–neuron interaction.[3]

The membrane of an acetylcholine neuron also contains special enzymes, so-called molecular scissors, cutting molecules of the spent neuromediator into fragments that re-enter synapses and get packed into vesicles and delivered along MTs back to the nucleus to be reconstituted [10, 11].

[1] See the Appendix for the list of abbreviations (p. 139).

[2] http//www.nobelprize.org/nobel_prizes/chemistry/laureates/1997/.

[3] Neuromediators are accumulated in vesicles due to the synchronous work of the motor (H^+ pump driving protons into vesicles) and the H^+/neuromediator exchanger.

Walking MMs carry mitochondria, besides neuromediators, from nuclei to periphery. Mitochondrial membranes contain other remarkable rotary electric motors/generators, F_0F_1-ATPases, producing by virtue of membrane potentials (~ 220 mV) the ATP molecules [2]. The membrane potentials themselves are generated as a result of glucose oxidation. An ATP serves as a source of energy needed for kinesin and other transporters to operate, for the growth of MT and lengthening of dendrites, for K^+ and Na^+ ion trafficking across the membranes, and membrane potential generation for the maintenance of neuronal activity and the build-up of new connections in the brain.

Hundreds of articles on MM experiments have been published in the past decade. They report the extensive use of such physical instruments and methods as X-ray crystallography, cryogenic electron microscopy, laser tweezers, and Q-DOT videos. In addition to references to concrete articles and reviews, we report below websites of leading laboratories having many years of experience with experimental and theoretical research in the field of interest [12–16].

Let us mention briefly estimates of neuron and brain energetics before considering the stochastic dynamics of intraneuronal transport.

1.3 Briefly about neuron and brain energetics

To recall, the membrane of a neuron is polarized, having excess K^+ ions on the inside, and Na^+ on the outside. The resting membrane potential is -70 mV. A stimulus (electric potential exceeding the threshold) induces ion currents across the membrane and a stereotypical change of the transmembrane potential, the so-called action potential with an amplitude of ~ 100 mV and duration around 2–5 ms. An approximate time scan of a typical action potential is presented in Fig. 1. This process is mathematically described by Hodgkin–Huxley equations or their rough analog, the FitzHugh–Nagumo model (see, for instance, monographs [17, 18]). In active transmembrane transport, ions are transferred across the membrane by a molecular ATP-powered pump (Na^+, K^+-ATPase).

Other MMs playing a fundamental role in neuronal function are also supplied by energy from interactions with adenosine-5′-triphosphate (ATP) molecules.

Every day, as many as $\sim 10^{26}$ ATP molecules or 10^{21} molecules per second are synthesized and consumed in the normal human body (which corresponds to ~ 50 kg or an energy of 2500 kJ). In the average, a neuron utilizes some $10^9 - 10^{10}$ molecules per second. Most of the neuron membrane ATP energy is spent to support MM operation, i.e., the work of the Na^+, K^+-ATPase pump (its mathematical model is not considered in this review).

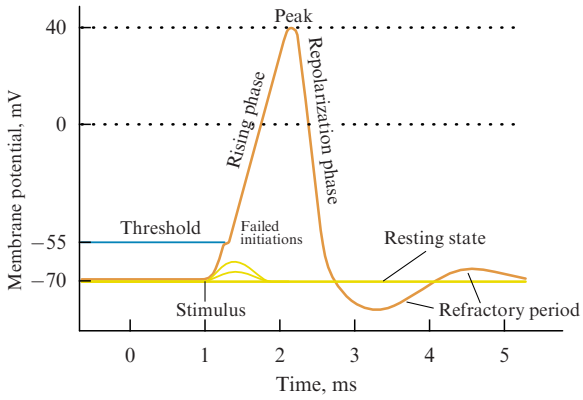

Figure 1. (Color online.) Approximate plot of a typical action potential.

In what follows, we report new averaged data on the energy consumed by neurons [19]. It should be mentioned first that human brain neurons generate approximately 10 nerve impulses per second. The energy utilized in a concrete cellular process in the brain cortex is distributed so that about 20% is spent on resting potentials, 21% on action potentials, and 59% on synaptic processes [including postsynaptic receptors — 50%, recirculation of neuromediators (neurotransmitters) — 4%, presynaptic Ca^{2+} inflow and vesicle circulation — 5%]. In other words, some 5–10% of the total energy consumed by MMs in neurons is spent to support the intraneuronal transport.

It is worthwhile to mark differential utilization of energy in selected brain regions. Specifically, cerebellar neurons spend 54% of their energy to maintain resting potentials, 22% on postsynaptic receptors, and only 17% on the generation of action potentials.

Experimental methods developed in recent decades make it possible to evaluate glucose consumption by different brain structures. One of them uses radioactive labels [20]. Glucose containing ^{14}C isotope in one or more of its carbons instead of the normal ^{12}C was administered to rats. The animals were rapidly frozen within 1 hour after injection, and ^{14}C radioactivity was measured in their brain sections. It was shown that the brain utilizes 30% of administered glucose. The authors who studied oxygen consumption in human organs arrived at a similar conclusion [21]. Verified data for the human brain are reported in Ref. [19].

1.4 General scheme of intraneuronal trafficking (as exemplified by acetylcholine-mediated neuromuscular transmission)

Figure 2 illustrates a diagram of a neuron cell with a long axon extending toward muscle fibers. (See, for example, Ref. [10] for a more detailed description of such a neuron.)

Figure 3a shows schematically a synaptic terminal, MT, and a network of actin filaments (AF). ‘Containers’ delivered by kinesins along MTs are reloaded onto the ‘heads’ of myosin V. The cargoes are exemplified by vesicles containing neuromediator molecules of acetylcholine (ACh) (shown by dumbbells) and their choline fragments (circles). The containers (synaptic vesicles) eject ACh molecules into the synaptic cleft when the membrane is electrically excited. The ACh molecules bind to membrane receptors of the target cell and thereby stimulate generation of the impulse.

This process completed, the neuromediator must by no means remain in the cleft. Otherwise, the next impulse (characteristic frequency of impulse arrival at the membrane being ~ 10 Hz) will cause ejection of a new portion of the neuromediator and the receptors will not be able to bind its excessive amount. The situation is saved by AChE, a hydrolytic enzyme acting as ‘molecular scissors’. It rapidly cuts ACh into halves, thus giving rise to acetate (A) and choline (Ch) fragments. The latter re-enter containers that are transported by MM dyneins to the nucleus for re-processing. The work of AChE is illustrated by Fig. 3b. Note that the other fragment, i.e., acetate, is always present in large enough amounts in neuroplasm [22].

ACh penetrates into the ‘throat’ of the active center (AC) as a result of diffusion and the effect of the electrostatic field

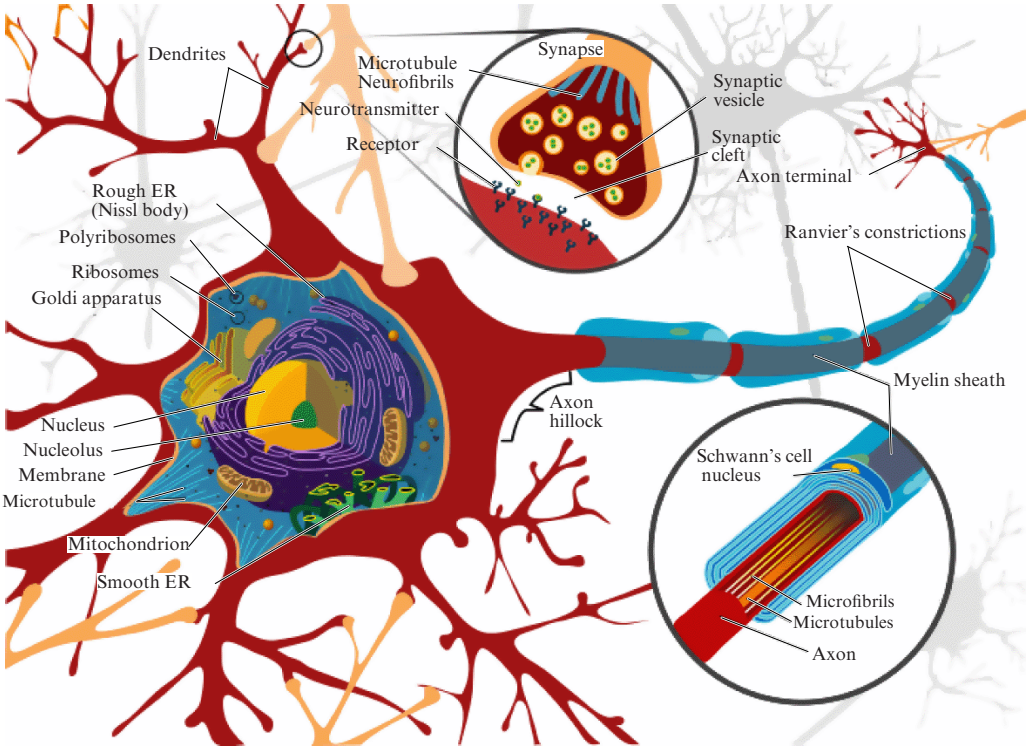

Figure 2. (Color online.) Complete neuron cell diagram (taken from Wikimedia Commons [Mariana Ruiz Villarreal]); ER — endoplasmic reticulum.

created by an AChE molecule. There, it gets attached to serine (Ser) and histidine (His) amino acid residues. An oxygen ion executing heat fluctuations attacks the chemical bond (thin line intersects bond in Fig. 3b), loosens it, and thereby triggers the ACh $\rightarrow$ A + Ch reaction. Then, the products are packed into vesicles again and the process continues. Notice that the action of neuroparalytic agents proceeds primarily through the AChE inhibition, when the nervous system is blocked by its own 'drug', and the organism dies. The active centers of MMs always contain groups playing the role of molecular scissors that cut an ATP molecule into adenosine diphosphate (ADP) and phosphate (P^-); these fragments leave the AC. Molecular scissors models are explored by the methods of molecular dynamics and quantum mechanics [23–25].

1.5 Molecular motors: kinesin, myosin V, and dynein

The legend to Fig. 4 showing MM 'images' provides details about distances between ACs on MTs or AFs that give kinesin, dynein, and myosin V 'steps'. It will be demonstrated in the next sections that regular processive 'stepping' of these MMs is not obligatory. Interstep time intervals depend predominantly on the local ATP concentration in neuroplasm, ATP hydrolysis time in the AC, and the time of reaction product release from the AC pocket. Naturally, one ATP molecule is needed to take a step.

The relevant cluster mathematical models of kinesin, myosin V, and dynein operating under random influences are considered in Sections 2.3, 3.2, and 4.3. It is these mathematical models that reveal the general principles underlying MM action.

Construction of a cluster MM model begins from the elucidation of MM spatial structure by X-ray diffraction analysis that permits differentiating between various functional states of MMs. Electron fluorescence microscopy methods are finding increasingly wider application in addition to X-ray imaging. Roentgenograms are corrected using molecular dynamics methods. The Protein Data Bank (PDB) stores information on hundreds of protein structures An article published in *Physics Uspekhi* highlights the multiplicity of structural forms of a remarkable MM, F_0F_1-ATPase [2], wherein the F_0 and F_1 complexes have been revealed. In turn, the latter consists of 9 protein subglobules. A similar scheme is used in Sections 2.1, 3.1, and 4.1 to describe the structure of other MMs, viz, kinesin, myosin V, and dynein, respectively.

2. How kinesin works

2.1 Functional scheme of kinesin

The kinesin molecule is a dimer composed of two identical polypeptide chains. One side of either chain harbors a $7.5 \times 4.5 \times 4.5$ -nm globular kinesin 'head' (KH) and a long 'tail'. The tails of the two monomer chains intertwine in opposite directions to be set on KH and form a fork that interacts with a tubuline-containing MT along which kinesin moves. One step of kinesin measures around 8 nm, i.e., exactly the size of two tubulin monomer globules that make up an MT. Kinesin usually takes 100 steps (800 nm) per second before it detaches completely from the MT. Kinesin stepping patterns are illustrated in Fig. 5, which also presents high-resolution stepping records over the timescale.

Two KHs are joined through a neck linker and form a stalk to which cargo can attach. The rigid connection between a KH and MT takes place when the KH active center is unoccupied. As an ATP molecule enters the active center, the torque exerting in the front KH causes an 8-nm advance of the rear KH. Then, the ATP molecule undergoes hydrolysis in the AC and decomposes into ADP and P^-, P leaves the AC, and the process repeats itself.

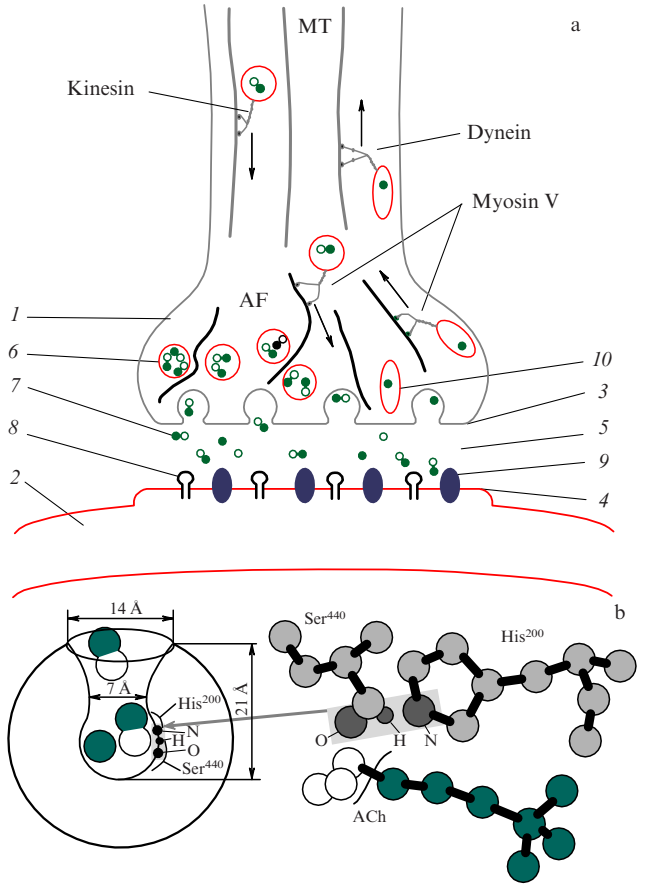

Figure 3. (Color online.) (a) Schematic of the nerve impulse transmission in a chemical synapse: *1* — presynaptic neuron terminal, *2* — postsynaptic neuron or target cell, *3* — presynaptic membrane, *4* — postsynaptic membrane, *5* — synaptic cleft, *6* — vesicles containing neuromediator (acetylcholine), *7* — released neuromediator, *8* — acetylcholine (ACh) receptors, *9* — acetylcholine esterase (AChE), and *10* — choline (Ch)-containing vesicles. (b) Schematic representation of an AChE molecule: dumbbell-shaped ACh molecules and disk-like acetyl (A) and choline molecules in the 'throat' of the active center connected with the AChE catalytic core. Thin line intersects the chemical bond ruptured.

Note that an MT provides 11 independent tracks along which cargo-laden kinesin molecules can move in parallel motion, overcoming Stokes drag (Fig. 4a).

The structure of many kinesins is known fairly well. Suffice it to mention up to 40 types of murine kinesins. There are a few open access animated movies demonstrating kinesin motion along MTs (see websites [12, 13]).

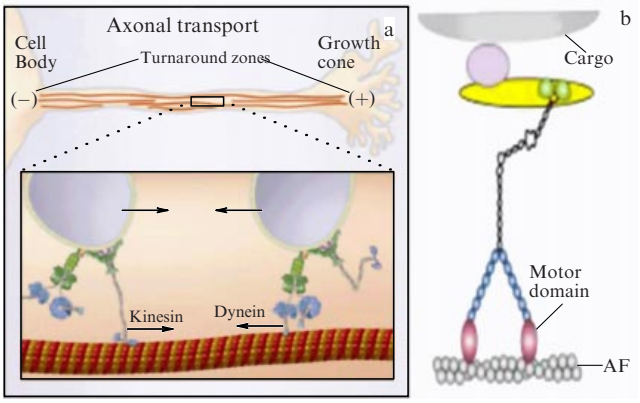

Figure 4. (Color online.) Molecular motors. (a) Forward (from cell nucleus) and backward transport along an MT. The former is mediated by kinesin, the latter by dynein (taken from Ref [26[). MT diameter ~ 25 nm. Distance between MT active centres ~ 16 nm. (b) Myosin V with a cargo on the actin filament ~ 7 nm in diameter. Distance between the 'heads' or motor domains of myosin V ~ 36 nm (taken from Ref. [27]).

Figure 6 shows the KH structure and MT cross section, together with the currently recognized scheme of events in the KH interacting with MT, ATP, and ADP molecules that give rise to a moment of force driving the cargo-laden stalk forward. This scheme is akin to a seesaw scheme.

The seesaw transmits force to the lever that moves cargo attached to the 'neck' along the MT toward its + end. The seesaw, in turn, is fastened to the MT. This contact breaks down after ATP decomposition, as the kinesin front head pulls the rear one. The head becomes detached, drawn forward together with the cargo and, being in diffusive motion, gets attached in front of the working head in the next potential well at the MT.

Figure 7 further explains previous figures by schematically illustrating kinesin stepping along a microtubule. Angle α describing the 'neck' position (see Fig. 6) is rotated through 180°; it is proportional to the slope of the CNB element in Fig. 7, or angle β in Fig. 6.

2.2 Evaluation of the energy needed to overcome Stokes' drag on a moving cargo

Let us assume that the torque remains unaltered from the instant of opening of angle β and pulling out of KH2 from the potential well, during further rotation of the cargo-laden neck ending in the attachment of KH2 in front of KH1, till the closure of angle β_1, while friction (drag) coefficients differ. In

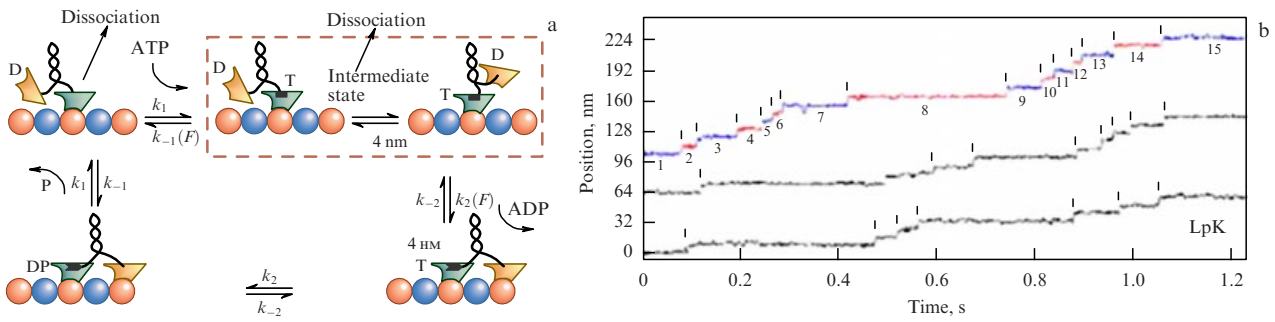

Figure 5. (Color online.) (a) Diagram illustrating motility of kinesin [28] (kinesin mechanochemical cycle). Notations inside the active center: T — ATP, D — ADP, and P — phosphate. (b) High-resolution stepping records of LpKbp kinesin from squid axons [29]. Vertical lines mark kinesin steps. The respective waiting intervals are numbered.

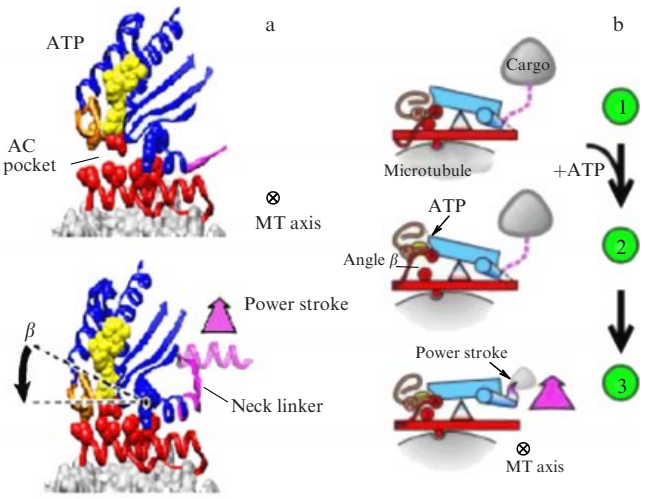

Figure 6. (Color online.) (a) Kinesin head molecular structure. (b) Events in the kinesin head interacting with an MT (taken from Ref. [30]). Arrows show the change in angle β. Symbol '$\times$' indicates the direction of forward motion along the MT. Angle β (slope) characterizes AC opening and varies from $\sim 30^\circ$ to 0° as ATP is sorbed on the AC pocket.

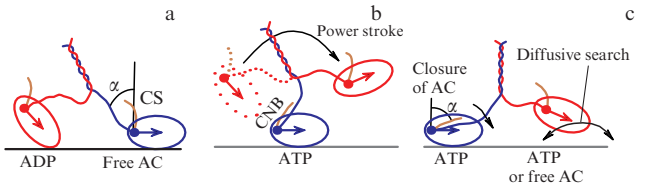

Figure 7. (Color online.) Stepping patterns of kinesin as it moves along a microtubule. (a) Release of P^- in the rear head results either in its dissociation or weakening of adhesion to the MT. (b) ATP binds to the leading head and thereby provides the power stroke by forming the CNB structure, promotes detachment of the rear head from MT, and moves it forward. CNB is an element equivalent to a seesaw arm. (c) The detached rear head moves diffusively together with the cargo in search of its binding site on the microtubule. Then the head, either weakly bound or free,'waits' for ADP to leave the active center. Thus, angle α varies from -90° (as shown in figure a) to $+90^\circ$ (figure c). Now, AC is prepared to admit ATP, and a new cycle is initiated (taken from Ref. [31]).

what follows, we take into account that the torque exerted from ATP sorption and closure of angle β is almost twice the torque changing angle α and advancing the cargo. The torque closing β_1 must at the same time open β_2 in KH2 and pull it out of the potential well.

It was shown in experiment that only half of the ATP energy is spent by kinesin to advance cargo. The other half is needed to pull out the rear KH (second 'foot'), draw it forward, etc. Therefore, we choose relevant estimates for the torques. We assume that torque $M(\beta)$ equals torque $M(\alpha)$ plus the pulling out torque, while the relatively small torque of Stokes force acting on the rear 'foot' being dragged is summed over with the torque overcoming the cargo's Stokes force.

Let us make appropriate estimates. Hydrolysis of ATP into ADP and P^- liberates an energy roughly equivalent to 40 J mol^{-1} or $\sim 15\,k_B T$ per ATP molecule, where k_B is the Boltzmann constant, and T is the temperature. As the leading KH moves the cargo approximately 8 nm with a force of 5 pN, it does work equaling 4×10^{-20} J (24 kJ mol^{-1} $\sim 20\,k_B T$), which means that only half of the ATP energy is spent to make a 'useful step'. Where does the other half go?

(1) *Losses related to dragging over the rear KH.* Let us assume that the cargo has a radius of 0.1 μm and the characteristic KH 'radius' is 3 nm $= 3\times10^{-3}$ μm, or two orders of magnitude shorter than the cargo radius. Therefore, the work done to drag over the rear KH detached from the MT is much smaller than that done to displace the cargo. Most likely, almost all additional efforts of the front KH are spent to detach the rear KH from the MT.

(2) Let us *estimate the build-up time of a single kinesin step* (or displacement of cargo a distance $L = 8$ nm). Let the cargo radius $r = 0.1$ μm. It follows from the Stokes law that

$$F = 6\pi r V \eta\,, \tag{1}$$

where F is the force of friction, $F = 6$ pN, η is the neuroplasm viscosity coefficient, $\eta = 20\times10^{-3}$ N s m^{-2} (protoplasm viscosity is 20 times that of water), V is the cargo speed, and step time τ^* is derived from equality $F\tau^* = 6\pi r\eta L$. Thus, $\tau^* \sim 50\times10^{-6}$ s. If r is longer, then τ^* is longer, too; vice versa, if $r = 0.01$ μm, τ^* is shorter: $\tau^* = 5\times10^{-6}$ s. The 'plateau' or step width being 1 ms, the step build-up time is 0.05 of its duration.

(3) Let us find now the *dimensional parameter* ς taking into account viscous drag and geometric characteristics of the system under consideration, making use of the above estimate of the time needed for angle β to decrease from 30° to 0°. We assume that the arm of force or the 'neck' for the cargo-moving torque is $L/2 = 4$ nm. Therefore, one has

$$\varsigma\,\mathrm{d}\alpha = F\,\frac{L}{2}\,\mathrm{d}t\,. \tag{2}$$

Reduction of β by $\pi/6$ results in an increase in α by π and $\varsigma\pi = F\tau^*(L/2)$. This gives the dimensional value of $\varsigma = FL\tau^*/(2\pi)$.

2.3 Mathematical model of kinesin walking

We construct a system of dynamic equations describing the interaction of two KHs by analogy with the system that describes rotor spinning in the molecular F_1-ATPase motor. The rotor spins under effect of torques generated in sequence by three identical β-subglobules as their ACs sorb ATP molecules [2, 32–35]. The three β-subglobules are linked via the rotor. Torques in the KH and their elastic strains are also created one after another as ATP molecules are sorbed in their ACs. KHs are connected by their neck linkers, and the torque exerted through the stalk advances the cargo along the MT (see Fig. 7). The set of equations describing a kinesin step (angle β_1 closes, and β_2 opens) looks like

$$\begin{aligned}
\varsigma\dot{\beta}_1 &= M(\beta_1) - \tau_1 + \varepsilon\dot{\beta}_2\,,\\
\mu\dot{\tau}_1 &= k\beta_1 - \tau_1\,,\\
\varsigma\dot{\beta}_2 &= M(\beta_2) - \tau_2 - \varepsilon\dot{\beta}_1\,,\\
\mu\dot{\tau}_2 &= k\beta_2 - \tau_2\,.
\end{aligned} \tag{3}$$

Here, $\beta_1(t)$ and $\beta_2(t)$ are the angles describing the closure of AC pockets in the KH in the course of ATP sorption, and $\tau_1(t)$ and $\tau_2(t)$ are elastic stresses arising from KH deformation. $\tau_1(t)$ and $\tau_2(t)$ lag behind elastic forces $k\beta_1$ and $k\beta_2$ due to ATP hydrolysis (decomposition) in the AC. $M(\beta_1)$ and $M(\beta_2)$ are the torques exerted in AC pockets undergoing deformation as they sorb ATP. To recall, angles β are proportional to α (see Fig. 7). The value of ς is a function of Stokes drag on the moving cargo, $\mu = \mu_1$ is the time of ATP

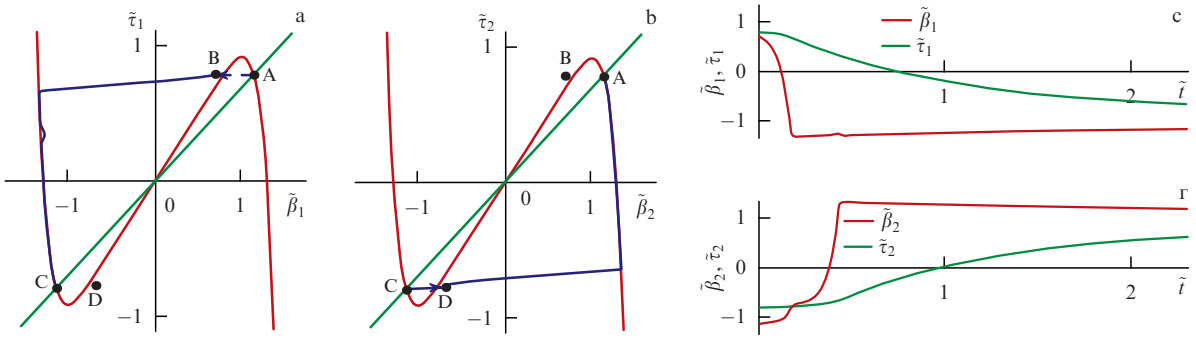

Figure 8. (Color online.) Phase planes $(\tilde{\beta}, \tilde{\tau})$ for the front (a) and rear (b) KH. Dark lines correspond to phase trajectories, light ones to the isoclines for system (4). (c, d) Graphs illustrating time dependences of angles and stresses for a single kinesin step shown on the phase planes. The jump in trajectory $\tilde{\beta}_2$ corresponds to the transition from C to D related to KH2 detachment from MT.

hydrolysis associated with AC pocket closure, and $\mu = \mu_2$ is the time of reaction product release upon the opening of an AC pocket. For simplicity, we take $\mu_1 = \mu_2 = \mu$, with k standing for KH elasticity, and $\varepsilon \ll \varsigma$ for the small coefficient characterizing force-mediated coupling between the two motors.

The corresponding set of equations in dimensionless variables takes the form

$$\begin{aligned}
\tilde{\varsigma}\dot{\tilde{\beta}}_1 &= \tilde{M}(\tilde{\beta}_1) - \tilde{\tau}_1 + \tilde{\varepsilon}\dot{\tilde{\beta}}_2\,,\\
\dot{\tilde{\tau}}_1 &= \tilde{k}\tilde{\beta}_1 - \tilde{\tau}_1\,,\\
\tilde{\varsigma}\dot{\tilde{\beta}}_2 &= \tilde{M}(\tilde{\beta}_2) - \tilde{\tau}_2 - \tilde{\varepsilon}\dot{\tilde{\beta}}_1\,,\\
\dot{\tilde{\tau}}_2 &= \tilde{k}\tilde{\beta}_2 - \tilde{\tau}_2\,,
\end{aligned} \tag{4}$$

where the relationship between kinesin kinematic angles $\beta_{1,2}$ and the respective dimensionless phase variables of the system of equations is described by the formula

$$\beta_i = \frac{\pi}{12}\,(\tilde{\beta}_i + 1)\,, \quad i = 1, 2\,. \tag{5}$$

The torque determined by ATF sorption forces or hydrolysis products (ADP and inorganic phosphate P^-) in KH active centers is given by the formula

$$\tilde{M}(\tilde{\beta}) = \tilde{\beta} - \frac{1}{n}\,\tilde{\beta}^n\,, \quad n = 3, 5, 7, \ldots\,, \tag{6}$$

with $\tilde{M}(\tilde{\beta}) = M(\beta)/M_0$, where M_0 is the maximum torque of forces ($M(\beta)$ becomes approximately N-shaped at large n). Other dimensionless variables are defined by the expressions

$$\tilde{t} = \frac{t}{\mu}\,, \quad \tilde{\varsigma} = \frac{\varsigma}{M_0\mu}\,, \quad \tilde{\tau} = \frac{\tau}{M_0}\,, \quad \tilde{k} = \frac{k}{M_0}\,, \quad \tilde{\varepsilon} = \frac{\varepsilon}{M_0\mu}\,. \tag{7}$$

Let us take, by way of example, numerical values of coefficients: $\mu = 5$ ms, $M_0 = 80$ pN nm, $\tilde{\varsigma} = 0.05$, $\tilde{k} = 0.7$, $\tilde{\varepsilon} = 0.015$, close to those in the F_1-ATPase model [2, 32]. The solution of system (4) is exemplified in Fig. 8 (see Ref. [36]).

Angle $\tilde{\beta}_1$ closes after sorption of an ATP molecule in the AC. It creates initial conditions at point B and the phase trajectory goes from B to C (Fig. 8a). The threshold (from C to D) needs to be surmounted for angle $\tilde{\beta}_2$ to open (Fig. 8b). This event can be promoted by the torque of force transferred from the front KH.

The transition from point A to point B at the phase plane of KH1 (Fig. 8a) corresponds to the arrival of ATP at the AC of the first (front) KH. Such a transition is somewhat delayed depending on ATP concentration in the medium. The delay is virtually unapparent in the presence of excess ATP, and stepping along MT occurs in a periodic manner (Fig. 9c, d). Phase planes corresponding to this case are displayed in Fig. 9a, b.

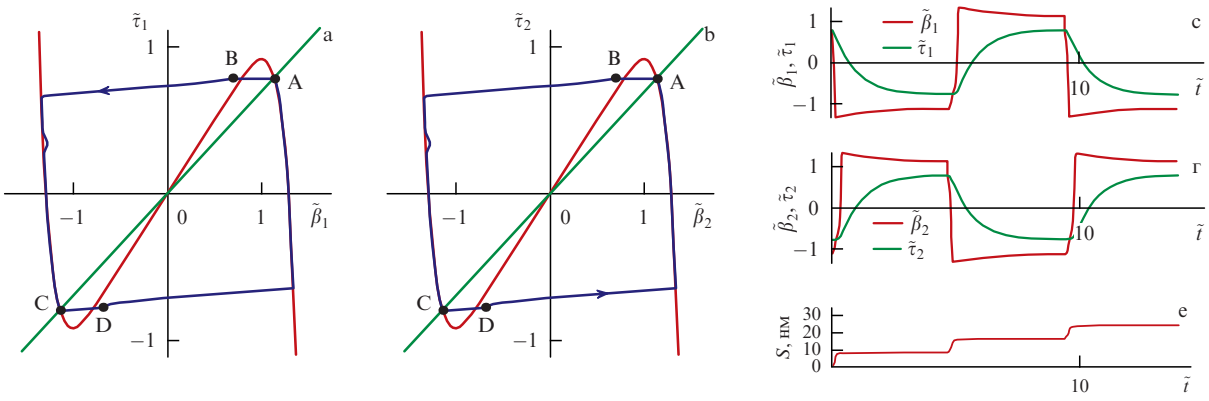

Figure 9. (Color online.) KH1 (a) and KH2 (b) trajectories on phase planes in the presence of ATP excess in a medium. Arrows indicate the direction of motion of the respective phase points along the trajectories. (c, d) Periodic (out of phase) changes in angles $\tilde{\beta}_1$ and $\tilde{\beta}_2$ and internal stresses $\tilde{\tau}_1$ and $\tilde{\tau}_2$ corresponding to kinesin steps in the presence of ATP excess in a mrdium shown on the phase planes. (e) Kinesin advancement along the MT corresponding to $\tilde{\beta}_1$ and $\tilde{\beta}_2$ changes. The distance covered is calculated as the sum of all 8-nm steps.

2.4 Comparison of model solutions and experimental data

Figure 10 compares calculated and observed stepping rates of kinesin moving along an MT.

It is worthwhile to emphasize again that the A–B transition (Fig. 9a) occurs only in association with ATP sorption in the AC. The appropriate transition probability depends on the ATP level in the medium. It was calculated based on the ATP diffusion coefficient in the medium, $\sim 1.5\times 10^{-10}$ m^2 s^{-1}, and the inlet hole area of the AC pocket, $\sim 2\times 10^{-19}$ m^2. Figure 11 presents results of modeling the kinesin steps at different ATP concentrations in the medium.

The authors of experiment [38] studied the dependence of the speed of movement of kinesin with the cargo in the form of a silicon dioxide bead (diameter 0.5 μm) along an MT on ATP molecule concentration. The bead motion was monitored using optical tweezers of variable force [37]. Our results are in qualitative agreement with the experimental data; namely, the speed of kinesin movement increases with a rise in ATP concentration and shows a tendency toward saturation. However, our calculations relate to a real case of cargo-bound kinesin movements *in vivo*, whereas *in vitro* experiments [38, 39] were carried out under a constant force exerted by laser tweezers.

This short discussion of the above solutions can be wound up with the following analogy. Cargo-bound kinesin stepping along an MT can be likened to a scuba diver walking over the silty bottom of a pond as he holds a cargo (water tank) in an outstretched hand. Since both the man and the cargo can be regarded as weightless, the entire work done by the former is for pulling the rear foot out of mud, as well as against Stokes drag. It is not known exactly how much energy is spent to advance the cargo and to pull out the foots.

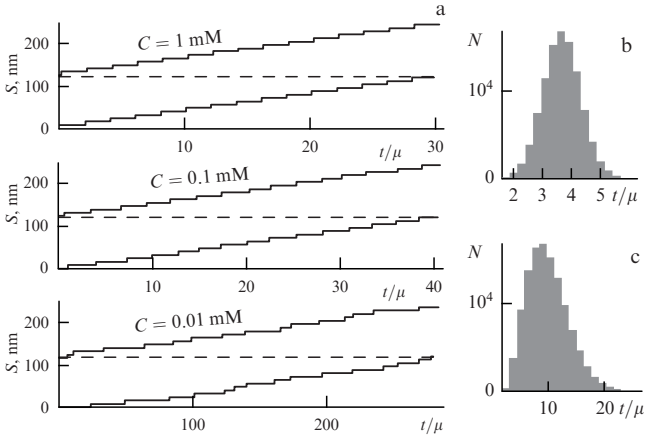

Figure 11. Results of simulation: (a) kinesin stepping scans at different ATP concentrations (delays related to the arrival of ATP at the kinesin AC are simulated by the Rayleigh distribution and depend on ATP concentrations in the medium); histograms of interstep time intervals at ATP concentrations of 0.1 mM (b) and 0.01 mM (c). Parameters of the model: $n = 11$, $\tilde{k} = 0.7$, $\tilde{\varsigma}_1 = \tilde{\varsigma}_2 = 0.002$, $\tilde{\varepsilon} = \tilde{\varepsilon}_2 = 0.0007$, and $\mu = 5$ ms.

3. Myosin V walking along actin filaments

3.1 Functional scheme of myosin V

Myosin motors have for a long time attracted the attention of researchers, since they play a key role in muscular motility [6]. In the sarcomeres of muscle cells, they work in concert to mediate sliding of actin filaments relative to one another. But myosin V, known already for 20 years as a molecular motor, is equally capable of stepping on its own along an AF. It is involved in trafficking neuromediators in synaptic terminals. Its stepping patterns are schematically presented in Fig. 12.

In what follows, angles Θ_1 and Θ_2 are the main variables considered (Fig. 12b). In the first approximation, Θ_1 is assumed to vary from 135° to 45° (or from $3\pi/4$ to $\pi/4$).

Importantly, hinge joint O and the cargo (Fig. 12b, c) move over fanlike surfaces, as in the case of kinesin, rather than in the drawing planes. The rear KH detached from the AF travels in a similar manner. Myosin V passes from state I into state III via surmounting the torque of Stokes drag on the cargo, the size of which is ten times the head size. This means that the basic step time for change in Θ_1 from 135° to 45° is determined by Stokes drag, whereas the search for a new contact of the detached rear head with the AF occurs in the course of fast diffusive motion.

It should be noted once again that both the force of the lever and the torque of elastic forces exerted by lever's deformation are used to advance the cargo (Fig. 12b) [40].

ATP sorption in the AC is accompanied by the closing of its pocket (angle β in Fig. 12d decreases), opening of the 'mouth', and head detachment from the AF. The hydrolysis of ATP in the AC and release of reaction products must occur to enable the mouth to close again upon a turn of the lever to the initial position. These processes take much more

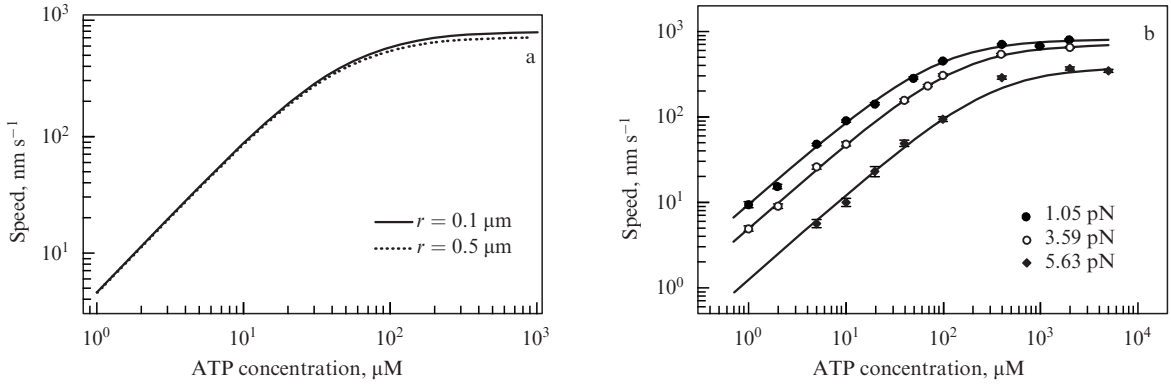

Figure 10. (a) Calculated stepping rate of kinesin moving along an MT at different ATP concentrations (r — radius of the transported cargo). (b) Experimental speed vs ATP concentration plots at different forces acting on the cargo [37].

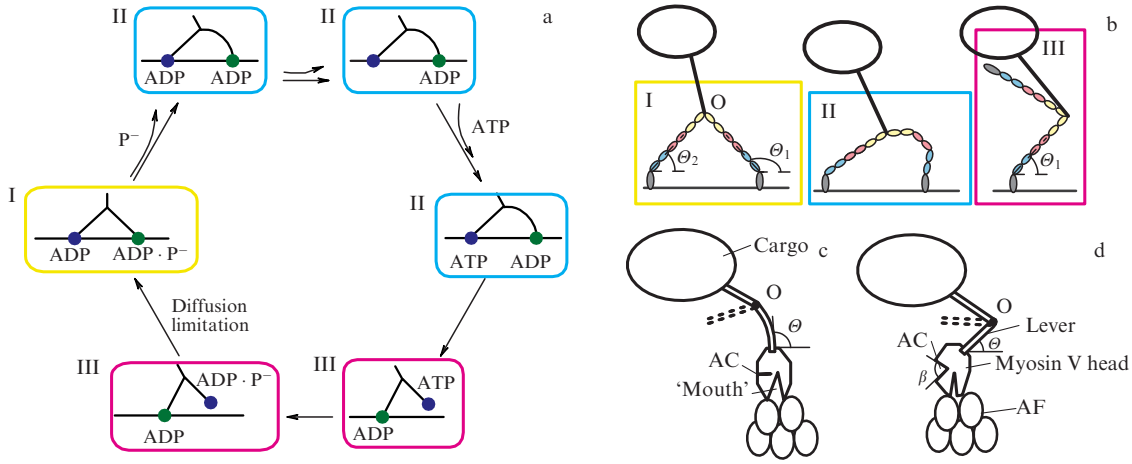

Figure 12. (Color online.) The mechanochemical cycle consistent with the kinetic myosin V model [40]: (a) transformations of ATP molecule in ACs of the front and rear heads (or motor domains) of myosin V, and (b) kinetic transitions of myosin V dimer cycling through three distinct mechanical states and cargo movement. Schematic interaction between the front head of myosin V and an actin filament (taken from Ref. [6]): (c) the head with the open 'mouth' is in contact with the actin filament, the lever is elastically strained, and (d) the AC head contains neither ATP nor reaction products, closing of the 'mouth' makes the lever turn and the cargo movement (taken from Ref. [40]).

time T than that needed to drag over the cargo, τ, that depends on the acting torque and the Stokes drag on the cargo. Thereafter, the cycle repeats itself for a new AF–head contact.

To sum up, the heads of myosin V operate alternately. After ATP hydrolysis is completed in the AC of the front head and it is relieved of reaction products, the mouth closes and becomes tightly attached to the AF. Elastic forces are now strong enough to detach the rear head from the AF, drag over the cargo attached to the hinge O through the rod connection (Fig. 12b), and make the rear head leapfrog over the leading one and re-attach in front of it. The rear head of myosin V, like that of kinesin, rapidly (for hundreds of picoseconds) finds via a diffusive search the new binding site ahead of the AF.

3.2 Initial parameter estimates and formulation of the myosin V walking model

Let us adopt the following estimates for the parameters of the myosin V walking model: (1) step length $l = 36$ nm, (2) mean longitudinal force F acting on the cargo and measured by laser tweezers is 1–2 pN, (3) energy expended on movement of the cargo is $W = Fl \sim 4 \times 10^{-20}$ J, and (4) length of the lever arm driving the cargo is $L = 20$ nm.

We believe that the force of action varies over the step length. The ATP energy, $W_{\mathrm{ATP}} = 30.5$ kJ mol$^{-1} \sim 5 \times 10^{20}$ J (see, for instance, review [2]). In other words, W_{ATP} is roughly 20% higher than expenditures on cargo movement.

Let us estimate the time of a single step or the 'substep front' (by analogy with kinesin). Taking account of expression (1) for the Stokes force exerted on the cargo yields the torque of Stokes force acting against the elastic forces when angle Θ_1 decreases:

$$M_{\mathrm{S}} = 6\pi r \, \frac{\mathrm{d}\Theta_1}{\mathrm{d}t} \, L^2 .$$

Let $r = 0.1$ μm, and $\eta = 20 \times 10^{-3}$ N s m^{-2}. Then, the time of step l is equal to

$$\tau = \frac{6\pi r l \eta}{F} \sim 1.5 \times 10^{-2} \text{ s} .$$

This expression disregards the short time for the diffusive search of the AF–rear head contact. The substep plateau duration is $\sim 5 \times 10^{-2}$ s [40] or much longer than the ATP hydrolysis time. It is actually the time of removal of ATP fragments (ADP and P$^-$) from the AC.

The energy of a stretched linear spring roughly modeling 'leg' bending is $W = K(\Delta x)^2/2 = 4 \times 10^{-20}$ J, where K is the spring stiffness coefficient. If $\Delta x = 0.5$ nm, then $K = 25 \times 10^{-2}$ N m^{-1}.

Since we do not know exactly how the angles of AC closing during ATP sorption are linked kinematically with the opening angle of the mouth or how the opening is related to the spring stress (additional compression or extension), it is therefore difficult to describe the relationship between the cargo-dragging torque and the torque exerted by a spring with poorly known characteristics. As a result, we have to directly estimate the effective elastic (strain) energy associated with a change in angle Θ in the front 'leg' that drags over the cargo as it turns through $\pi/2$.

The cargo-dragging torque is estimated at ~ 30 pN nm. This value is comparable with that for both ATPase and kinesin. Let us assume that the elastic energy spent on moving the cargo is

$$\frac{K(\Delta\Theta)^2}{2} = 0.8 \, W_{\mathrm{ATP}} = 4 \times 10^{-20} \text{ J} ,$$

$$(\Delta\Theta)^2 = \left(\frac{\pi}{2}\right)^2 \approx 2.5 .$$

Hence, $K = (8/2.5) \times 10^{-20}$ J rad^{-2}. Notice that such a value of the elasticity coefficient is smaller than the estimates for the F_1-ATPase model [2] and kinesin. In fact, the strain energy nonlinearly depends on Θ (see calculations in Ref. [40]). Bearing this in mind, a K value that two times higher can be taken for semi-qualitative estimations.

The substep plateau duration gives the approximate value of the parameter $\mu \sim 50$ ms. The Stokes force torque exerted on the cargo against the elastic force torque is given by

$$M_1 = 6\pi r V \eta L = 6\pi r \, \frac{\mathrm{d}\Theta_1}{\mathrm{d}t} \, L^2 \eta = \varsigma_1 \, \frac{\mathrm{d}\Theta_1}{\mathrm{d}t} .$$

The Stokes force torque related to the stored elastic energy assumes the form

$$M_2 = 6\pi(0.1r)\,\frac{\mathrm{d}\Theta_2}{\mathrm{d}t}\,L^2\eta = \varsigma_2\,\frac{\mathrm{d}\Theta_2}{\mathrm{d}t} = 0.1\varsigma_1\,\frac{\mathrm{d}\Theta_2}{\mathrm{d}t}\,.$$

We take, as in the case of kinesin, $r = 0.1$ μm and $\eta = 20\times10^{-3}$ N s m^{-2}. Then, estimates give $\varsigma_1 \sim 3\times10^{-23}$ N s m, and $\varsigma_2 \sim 3\times10^{-24}$ N s m.

The introduction of dimensionless time and other dimensionless quantities, as for kinesin [see formula (7)], viz.

$$\tilde{t} = \frac{t}{\mu}\,,\quad \tilde{\varsigma}_i = \frac{\varsigma_i}{M_0\mu}\,,\quad \tilde{\tau}_i = \frac{\tau_i}{M_0}\,,\quad \tilde{k} = \frac{K}{M_0}\,,\quad i = 1,2$$

(where M_0 varies from 40 to 80 pN nm), yields the following set of equations in dimensionless variables for a single step of myosin V:

$$\begin{aligned}
&\tilde{\varsigma}_1\dot{\tilde{\beta}}_1 = \tilde{M}(\tilde{\beta}_1) - \tilde{\tau}_1 - \tilde{\varepsilon}_1\dot{\tilde{\beta}}_2\,,\\
&\dot{\tilde{\tau}}_1 = \tilde{k}\tilde{\beta}_1 - \tilde{\tau}_1\,,\\
&\tilde{\varsigma}_2\dot{\tilde{\beta}}_2 = \tilde{M}(\tilde{\beta}_2) - \tilde{\tau}_2 + \tilde{\varepsilon}_2\dot{\tilde{\beta}}_1\,,\\
&\dot{\tilde{\tau}}_2 = \tilde{k}\tilde{\beta}_2 - \tilde{\tau}_2\,.
\end{aligned} \tag{8}$$

Here, the relationship between kinematic angles of myosin V and dimensionless phase variables of the set of equations is described by the formula

$$\Theta_i = \frac{\pi}{4}\,(2 - \tilde{\beta}_i)\,,\quad i = 1,2\,. \tag{9}$$

Accordingly, Θ_1 decreases from $3\pi/4$ to $\pi/4$ and Θ_2 from $\pi/4$ to $3\pi/4$ in the course of a step time. Then, Θ_1 and Θ_2 change places. Torque of force $\tilde{M}(\tilde{\beta})$ is given by formula (6). The values of the dimensionless coefficients of the system are computed based on the estimates of the respective dimensional parameters obtained in this section.

3.3 Results of modeling the myosin V walking and comparison with experiment

Phase planes of the model and unfolded solutions for interacting motor domains or myosin V heads (MHs, see Fig. 12) are presented in Figs 13 and 14. In Fig. 13a, b, the solutions or image point movements on the phase planes are marked by the dark line. In the case of slow movements, they practically coincide with the branches of the principal isoclines (light lines) due to the relaxation behavior of the system.

The passage of a phase image point over the barrier (from A to B) is possible only after ATP arrives at the open AC of the rear 'leg', the AC pocket closes, the mouth opens, and the energy is stored as Θ_B changes from $\pi/4$ to $3\pi/4$, while Stokes work is very small in the process.

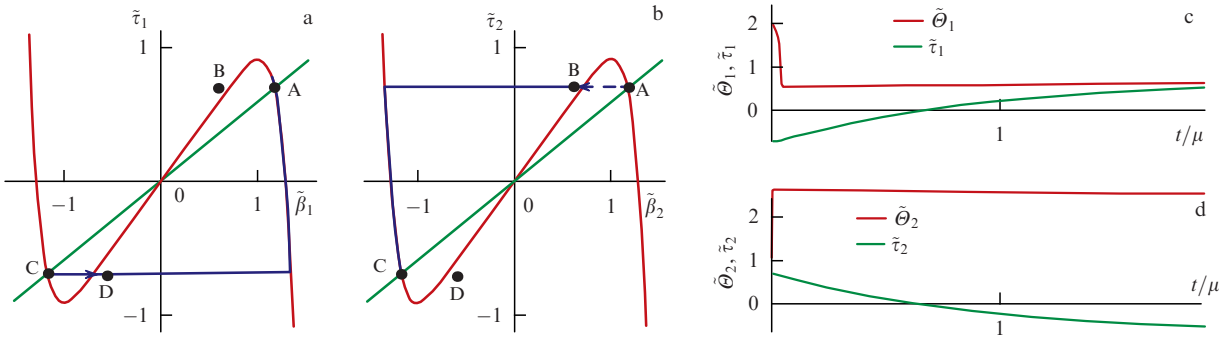

Figure 13. (Color online.) Trajectories of myosin V stepping over MH1 (a) and MH2 (b) phase planes. Out of phase changes of angles Θ_1 (c) and Θ_2 (d) and internal stresses corresponding to a single myosin V step shown on MH1 and MH2 phase planes ($\mu = 50$ ms).

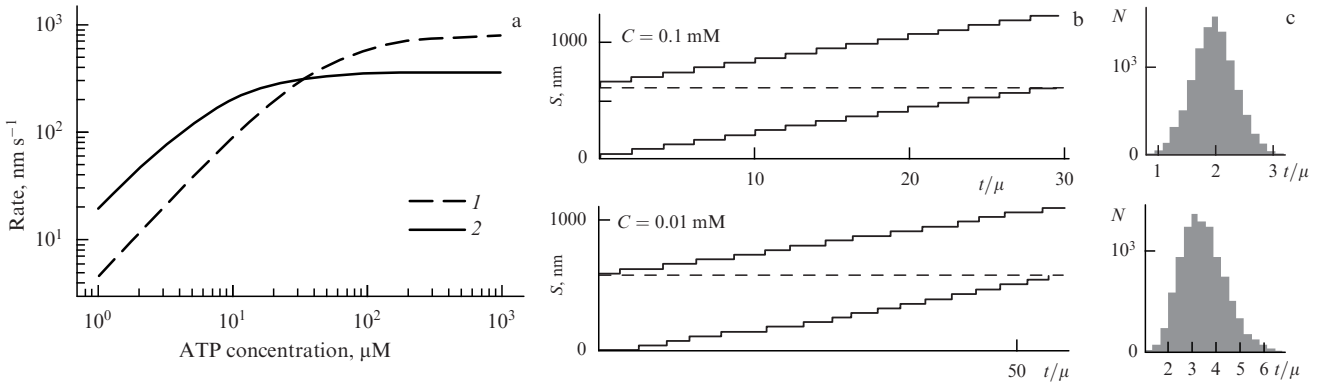

Figure 14. (a) Calculated stepping rate of myosin V on actin filaments depending on ATP concentration (curve *1*); for comparison, kinesin stepping rate on MTs is shown (curve *2*). In both cases, the cargo radius $r = 0.1$ μm. Parameters of the model: $L = 20$ nm, $n = 11$, $\tilde{k} = 0.6$, $\tilde{\varsigma}_1 = 0.015$, $\tilde{\varsigma}_2 = 0.0015$, $\varepsilon_1 = 0.005$, $\tilde{\varepsilon}_2 = 0.0005$, and $\mu = 50$ ms. Myosin V stepping scans (b) and histograms of interstep time intervals (c) at ATP concentrations of 0.1 mM (top) and 0.01 mM (bottom), with $\mu = 50$ ms. Delays related to ATP arrival at the myosin V AC are simulated by the Rayleigh distribution and depend on ATP levels in the medium.

The stored 'elastic' energy released during a step (transition from point C to D) is spent to drag over the cargo and pull the rear 'leg' (or head) of myosin V out of the potential well on the AF.

The main difference between kinesin and myosin V models consists in the following. ATP sorption in the kinesin AC generates a torque dragging over the cargo against Stokes forces. ATP sorption in the myosin V AC results in the storage of elastic energy. Internal Stokes drag losses are small here. The stored elastic strain energy is expended in myosin V stepping and cargo movement.

4. Dynein

4.1 Functional scheme of dynein

Dynein is one more remarkable molecular motor performing a variety of functions in living cells. In fact, it is one of the most important motors walking along MTs in neurons (see Fig. 4). It operates in the ensemble with other motors that collectively maintain the mobility of flagella and also participates in generating mitotic forces. To recall, myosin is also a component in sarcomere organization responsible for muscle function and ameboid motility.

The structure of dynein and the mechanism behind its step-by-step walking along MTs are considered below as exemplified by dyneins operating in mammalian cells (especially neurons) where they make the most regular movements. Dyneins in yeast and ameboid cells exhibit a more intricate walking behavior.

It should be noted both the difference and similarity in the work of kinesin and dynein. The former consists in the fact that kinesin steps along a single track of an MT, from its '−' end to the '+' one, while dynein uses two tracks and travels in opposite directions. The latter is that the cargo size is in either case much greater than the MM size (Fig. 4).

The dynein motor (Fig. 15a) is comprised of two identical disk-shaped drivers each connected with the tail by a lever (linker) and a neck. The lever is roughly 13 nm long. The loose ends of two tails are tied up and can be attached to a cargo, e.g., a vesicle with neuromediator fragments, via intermediate proteins (see Fig. 3a). The driver can be connected to the AC on an MT via the 'leg' (stalk) with the 'foot' domain.

The main part of the dynein motor is a hexahedron or a 4-nm thick disk some 10 nm in diameter. Each of its AAA links is formed by two subglobules (Fig. 15b) separated by an AC capable of admitting an ATP molecule. Its sorption capacity makes the 'mouth' (a gap between subglobules) close. This structure resembles that of other ATPase-driven motors, viz. kinesin, myosin V, and F_1-ATPase (see Refs [26, 41]). However, these approving subglobules transmit force onto the lever through the ArgFinger only in the AAA1 domain, thus making the lever bend through angle α. This domain, in particular, plays the key role in the dynein motor. The lever bend angle is approximately 90°. Such strain is associated with the storage of elastic energy. Both the leg and the neck connecting the linker with the tail appear to be involved in energy storage (the situation is reminiscent of that described above for myosin V). The foot is detached from the active center of the MT, with the force from the partner motor being transmitted through the leg. This implies consumption of part of the ATP sorption energy.

To conclude, the energy contribution in dynein, similar to kinesin, myosin V, and F_1-ATPase, is mediated through ATP sorption. However, the torque of forces exerted by ATP sorption in the AC of kinesin and F_1-ATPase is directly transmitted to the actuator, i.e., the rotor in F_1-ATPase or the neck dragging over cargo in kinesin. On the other hand, in the AC of myosin V and dynein, the energy is first stored in elastic strain. The role of the remaining elements of the AAA+ hexahedron remains to be clarified. They may participate in linker fixation in the stressed state.

All states of the dynein motor in different phases of its working cycle are shown in Fig. 16.

4.2 Dynein walking experiments

Figure 17 summarizes experimental data on dynein movements along MT microchannels based largely on the studies made in R.D. Vale Lab [12].

Kinesin and myosin V take alternating steps along a single MT microchannel or AF. In contrast, dynein makes use of two parallel microchannels at a time. Its movement in a step-

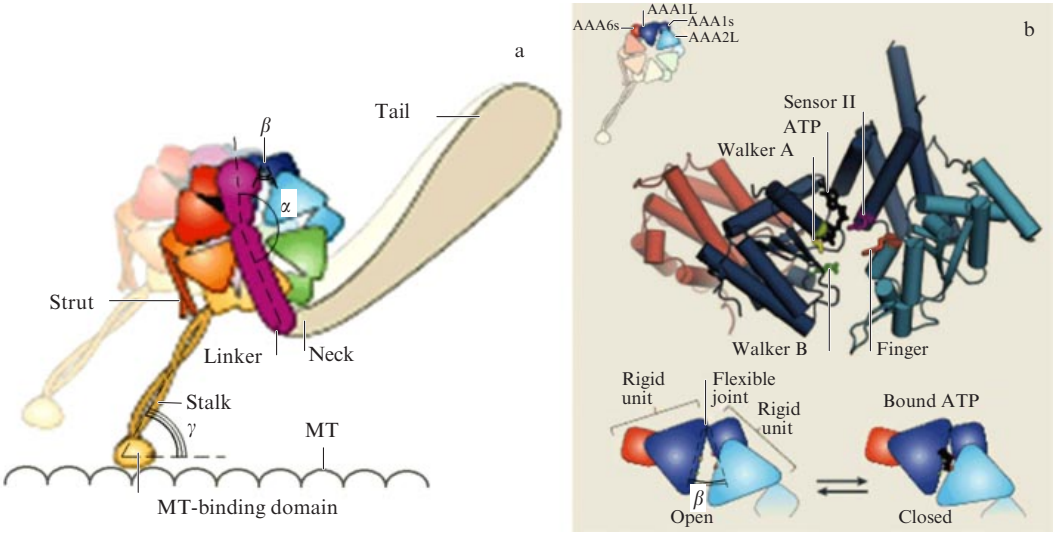

Figure 15. (Color online.) Overview of dynein composition (a) and its active center (b). Characteristic dimensions: MT-binding domain ('foot') — 5 nm, 'leg' ('stalk') — 10 nm, and lever (linker) — 13–14 nm [7].

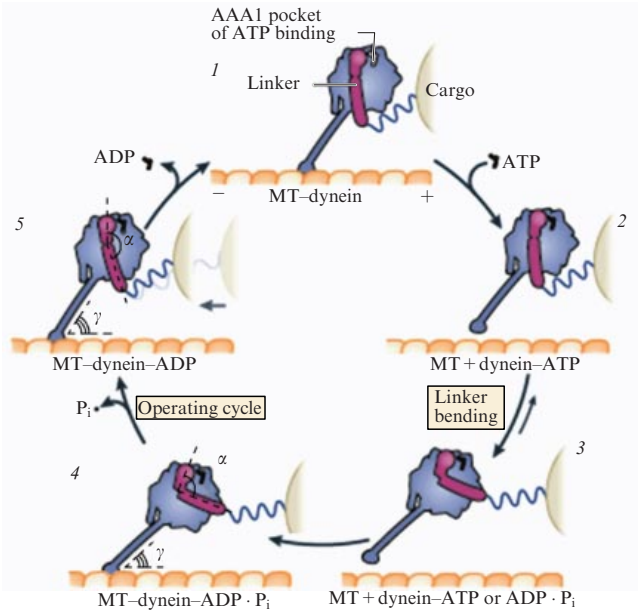

Figure 16. (Color online.) Dynein motor states in different phases of the working cycle: *1* — active center free of nucleotides (ATP and ADP), 'foot' bound to an MT active center; *2*, *3* — ATP entering active center, 'linker' undergoes deformation, 'foot' is liberated from the AC of an MT; *4*, *5* — as a result of Brownian motion, the 'leg' binds to the next AC on the MT. Active products of hydrolysis are released from the AC (first, phosphate P-, then ADP).The linker straightens and trails cargo after it [7, 42].

by-step fashion prevails but is not restricted to this single mode of walking. For example, the right leg may take two steps, while the left leg skips one step or either leg can jump from one microchannel to the other. Such complex motion is typical of yeast dynein.

This stepping behavior is possible for two reasons. Dynein legs are much longer than in kinesin or myosin V and can exert a twisting moment. The legs walking along different microchannels are likely to hop from one to the other. As a result, an intricate path is followed. Certain dyneins have a more complicated structure that accounts for their motion along a straight line.

There is a variety of dynein motors. Vale and co-workers extracted dynein from yeast cultures and took MTs from neurons. (To recall, Vale discovered kinesin in extracts of neuroplasm from squid axons.)

All experimental data presented in Fig. 17 were obtained *in vitro* using a microscope with a laser beam that lighted up quantum dots on the stepping dynein once every 20 ms at an ATP concentration of 4 μM (note that the *in vivo* ATP level was 2 mM). In all probability, the choice of so low an ATP concentration was necessary to ensure a long interstep time (seconds).

As mentioned above, the time of the step itself is much shorter and depends on the cargo (its dimensions, to be precise).

Histograms illustrating interstep time spread, step size, stepping rate, and path length distributions of dynein walking

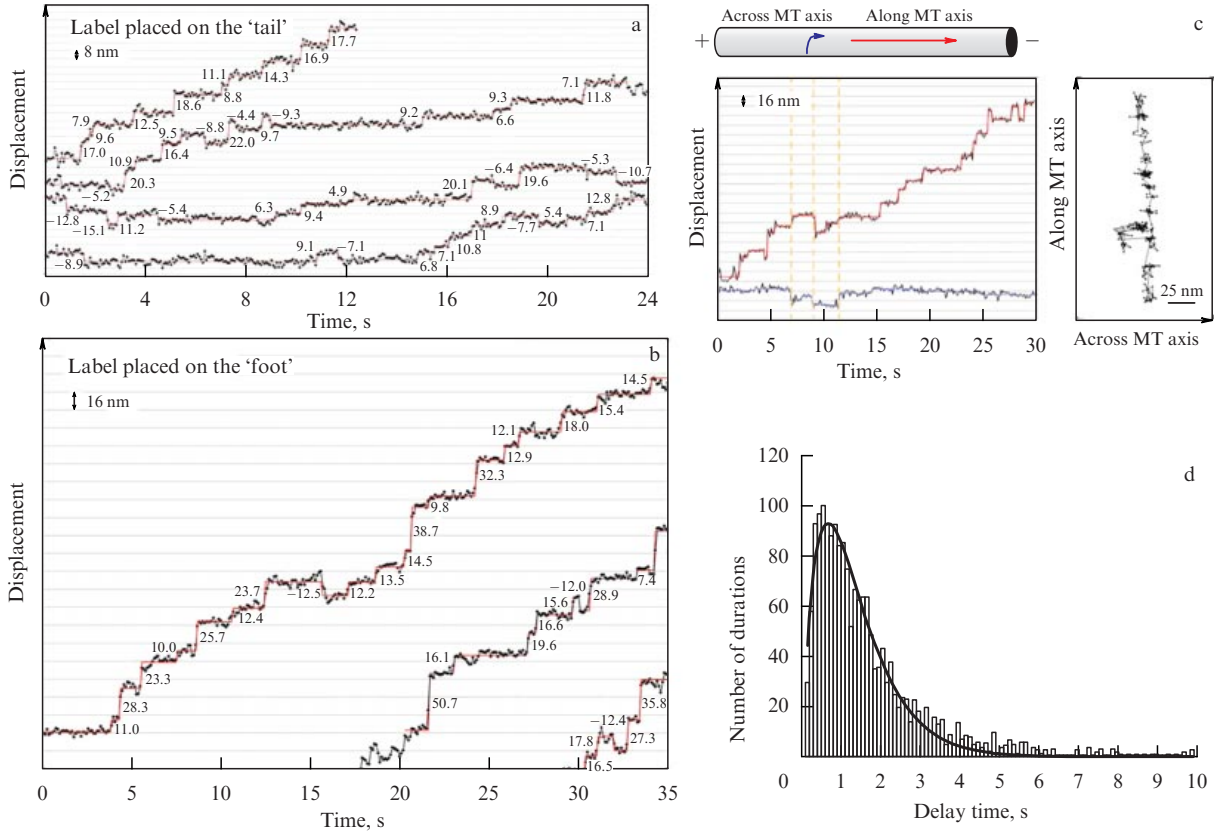

Figure 17. (Color online). Experimental stepping scans of dynein along an MT in the absence of a cargo. (a) Luminous fluorescent labels (quantum dots) placed on the end of the tail (shown in blue) correspond to the shift of the dynein center of mass. (b) Quantum dots labeling the domain involved in the leg movement. Therefore, the step size is ~ 8 nm in figure a, and ~ 16 nm in figure b. The automated microscope shutter through which the probing laser beam passed made it possible to light up the label every 20 ms (blue dots). The red line connecting these dots is derived using a special step-finding program [26]. (c) The path of dynein moving along and across an MT. (d) An example of the delay time distribution in dynein steps.

along an MT are presented in Refs [41, 42]. Backward steps were observed too, probably because dynein hopped from one MT microchannel to the other. ATP concentrations in the reported data being low, dynein stepping rates were much smaller than those of kinesin and myosin V maximum values.

We compared these experimental findings with our calculations based on the histogram presented in Fig. 17d that best of all corresponds to the conditions of our model in which dynein legs take alternating rectilinear steps. Equations (8) had to be substantially extended to simulate steps across MTs and backward steps.

4.3 Simple mathematical model of dynein with alternating steps

Let us proceed from the analogy of mathematical myosin V and dynein models considering ATP sorption in the AC open pocket (see Fig. 16).

If the pocket is empty ($\tilde{\beta} = +1$), the angle characterizing the linker position is $\alpha = \pi$; if the AC contains ATP ($\tilde{\beta} = -1$), $\alpha = \pi/2$. It is assumed that the linker bends due to its rigid kinematic connection with the AC pocket wall. Alternatively, $\alpha \sim \pi(\tilde{\beta} + 3)/4$, where α is the linker bend angle, with the angle between the leg and the MT (denoted by γ) being $\gamma \sim \pi(\tilde{\beta} + 3)/12$.

The operating cycle includes ATP hydrolysis followed by the removal of reaction products (ADP and P^-) from the AC and straightening of the linker (see Fig. 16). To recall, we describe the simplest case of dynein walking, when each leg makes alternating 16-nm steps along its specific track on the MC and the disk-like drivers move in parallel.

Let us assume, as in the case of myosin V, that elastic strain upon a change of angle α from π to $\pi/2$ is associated with the storage of energy

$$W_{\text{el}} = aW_{\text{ATP}}\,, \tag{10}$$

where the coefficient a indicates what part of the energy brought in by ATP sorption transforms into potential energy of the spring (the remaining part is lost as heat), $a \leqslant 1$.

If the 'spring' is linear as in the case with myosin V, then one finds

$$W_{\text{el}} = \frac{k(\Delta\alpha)^2}{2}. \tag{11}$$

According to results reported in papers [41, 42], dynein develops a force of 4–5 pN, meaning that its moment is $M \sim 40-80$ pN nm. Let us introduce corrections to Eqns (8). The cargo was absent in the above experiments. Therefore, $\tilde{\varsigma}_2$ is by an order of magnitude smaller than in myosin V. The coupling coefficients between drivers $\tilde{\varepsilon}_1$ and $\tilde{\varepsilon}_2$ should be selected. It is most important that since the ATP level is low, the probability of initiating each step is rather small. The product liberation time μ is the same as for myosin V.

The respective solution in dimensionless variables in the presence of excess ATP in the medium is represented in Fig. 18. In the situation being considered, the first step corresponds to the phase of dynein motion in which the linker is bent and the 'leg' of the first driver lifted (its 'foot' being detached from the MT), while the foot of the second driver is attached to the MT, the linker straightens, and the force transmitted through the 'leg' drags over dynein forward.

Simulation on the assumption of a low ATP concentration (4 μM) yields the result shown in Fig. 19. An example of similar experimental data (dynein stepping behavior on an MT) and the respective delay time histogram are presented in Fig. 17b, d. In this experiment, the advancement of the labelled head was recorded; in the average it was ∼ 16 nm, which is twofold greater than the advancement of the dynein center of mass for one step.

It should be emphasized once again that our model is of limited use, because it describes dynein walking with alternating steps along a straight line. A wealth of data from Vale's Lab [12] gives reason to presuppose other real situations where dynein steps across an MT, backward steps, etc. are taken into consideration, while dynein-transported cargo is disregarded. Therefore, the comparison of our calculations corresponding to the model taking account of the influence of the cargo with experimental statistics is of limited value.

Section 5 below deals with more general cases of dynein stepping behavior.

5. Alternative models of molecular motors

5.1 Dynein model and the Monte Carlo method

This section presents a new mathematical model of dynein, called the winch model by the authors [43]. It is reminiscent of

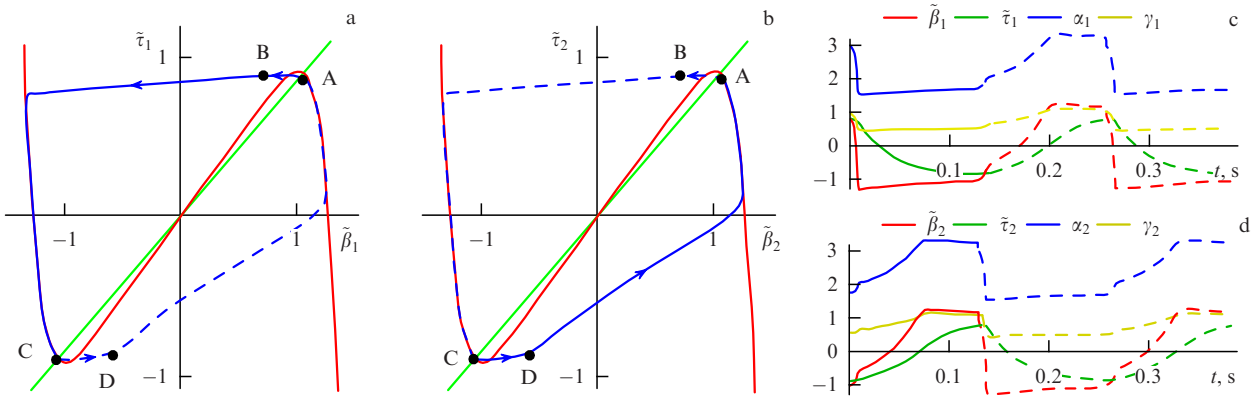

Figure 18. (Color online.) Results of mathematical modeling the step-by-step motion of dynein: curves on the phase planes ($\tilde{\beta}_1$, $\tilde{\tau}_1$) and ($\tilde{\beta}_2$, $\tilde{\tau}_2$) corresponding to the states of the first (a) and second (b) drivers of dynein, and (c, d) time dependences of these phase variables, linker bending angles, and angles between the 'legs' and the MT. Solid lines denote the first step, and dashed lines the following ones. Maximum ATP concentration, cargo diameter around 0.5 μm (corresponds to the size of a mitochondrion), $n = 11$, $\tilde{k} = 0.85$, $\tilde{\varsigma}_1 = 0.05$, $\tilde{\varepsilon}_1 = 0.01$, $\tilde{\varsigma}_2 = 0.5$, $\tilde{\varepsilon}_2 = 0.1$, $\mu = 50$ ms, $\alpha_i \sim \pi(\tilde{\beta}_i + 3)/4$, $\beta_i \sim \pi(\tilde{\beta}_i + 1)/12$, and $\gamma_i \sim \pi(\tilde{\beta}_i + 3)/12$, with $i = 1, 2$.

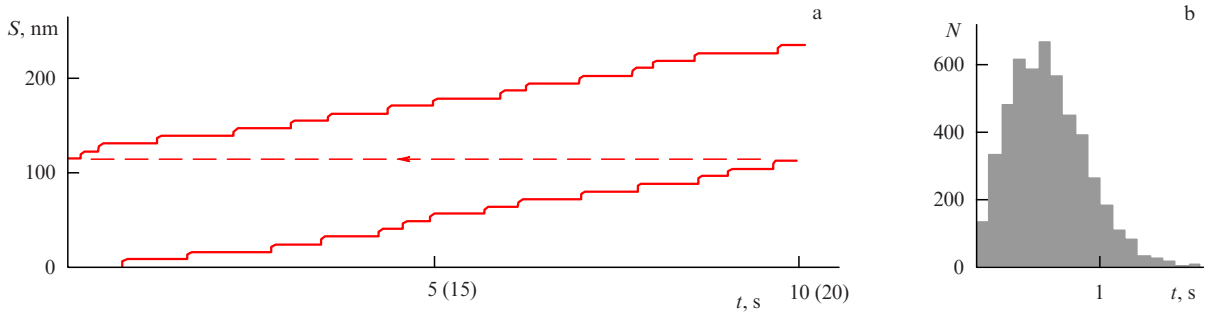

Figure 19. Results of mathematical modeling of dynein steps at ATP concentration of 0.004 mM (the molecule's center of mass advances 8 nm with each step).

the F_1-ATPase model proposed by Oster and co-workers [14, 35].

The first parameters evaluated in this model are potential energies of dynein states depending on the mutual positions of the two drivers tied up by the 'tails' and on the states of their AC, i.e., the absence of nucleotides or presence of ATP, ADP, etc. in the active centers. The latter states, in turn, depend on the position of the linkers of both motors. Moreover, the disk-to-disk coupling energy of these motors is calculated depending on their mutual positions.

The model thoroughly takes account of the potential elastic strain energy of dynein 'legs' for two angles and the torsion angle between the 'legs' that contact differently with the MT. It is the stress in the MT-bound front dynein leg that enables the rear one to detach from the MT after its AC sorbs ATP and exerts the driving torque dragging over the dynein. This probably accounts for the name 'winch model'.

Since legs are likely to deform, the motor disks cannot only move parallel to each other but also step aside, while the legs fall into neighboring microchannels. Such stepping behavior is inherent in yeast dynein. In neurons, disks usually move parallel to each other (Fig. 20). The authors argue that the state of a two-disk system in thermal equilibrium corresponds to an energy minimum

$$U = U_1 + U_2 + U_{\mathrm{INT}} + Fx\,, \tag{12}$$

where U_1 and U_2 are the potential energies stored in elastic strains of the 'legs' of the first and second motors, respec-

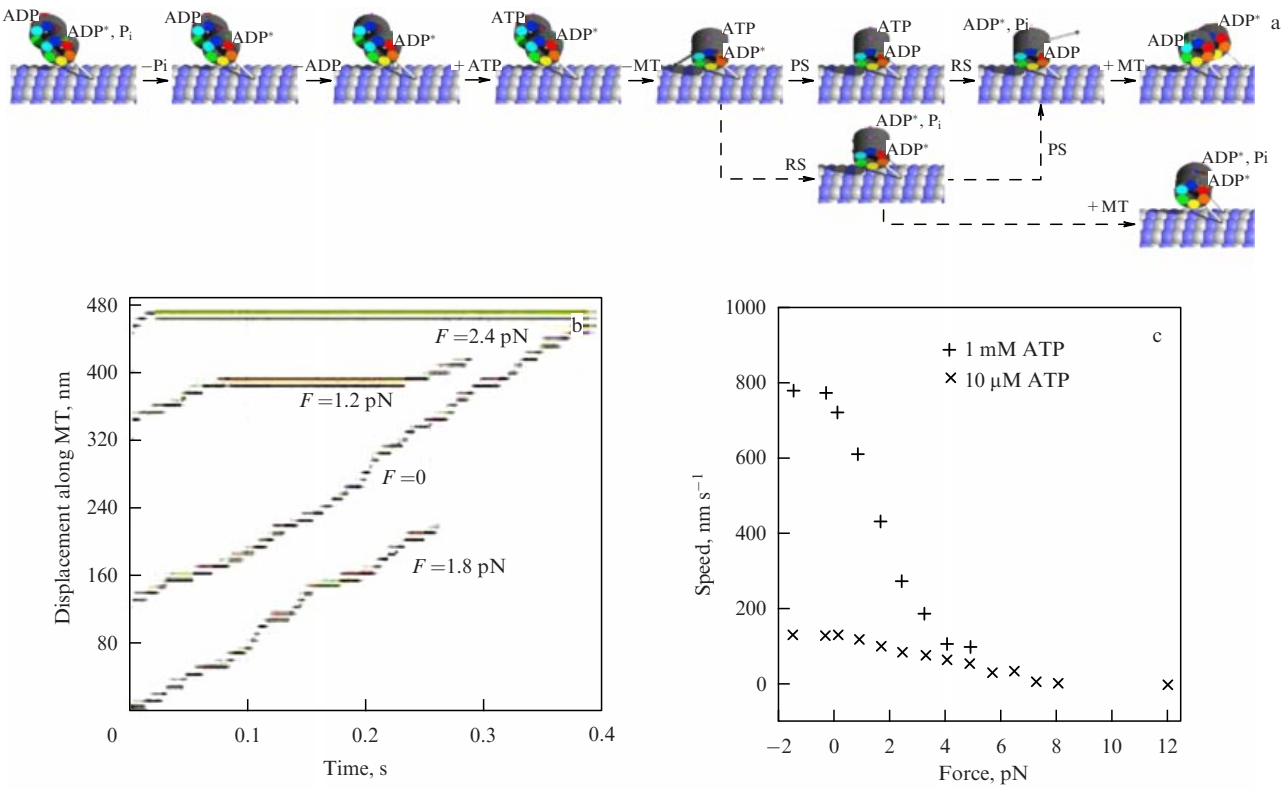

Figure 20. (Color online.) Dynein single-molecule kinetics of tightly coupled motors (after Fig. 5 in Ref. [43]). (a) The most probable kinetic pathways for a dimeric dynein molecule. The main path (continuous arrows) leads to an advancing step. If the binding of one leg occurs before the power stroke in its partner, this can lead to a futile step (dashed arrows). (b) A portion of the on-axis stepping trace of a dimeric dynein molecule for different values of the load. Trace of the tail of the dynein (black) and the corresponding x-coordinates of the left (red) and the right (green) feet are depicted. (c) Force–speed diagrams of walking dynein for two ATP concentrations (1 mM and 10 μM).

tively, $U_{\rm INT}$ is the potential energy of the tail–tail interaction proportional to the square of tail displacement with respect to the linkers and the potential energy of interaction between the motor disks with regard for the distance and turns relative to each other, Fx is the work done against force F applied parallel to the MT axis, and x is the displacement of the center of the section connecting linker joints. In calculations, force F varied from -1 to $+7$ pN.

The energy was calculated for a total of N states:

$$N = 5^2(1 + 2 + r)\,. \tag{13}$$

In so doing, dynein could be bound to MT via one or two 'legs', with $r = 34$ being the number of various positions of dynein disks relative to each other. Thus, a total of $N = 925$ states were considered. The minimum energies were calculated numerically by the Monte Carlo method. Figure 20 presents an example of a calculation for the simplest case of dynein whose motors step along parallel MTs.

The Appendix to Ref. [43] presents many examples of more complicated dynein movements and animations of dynein walk in different stepping modes. Coming back to our remark, it is worthwhile to note that the model being considered is conceptually related to the Fokker–Plank model [14, 35] defining the probability of transition from one state to another in a rotary F_1-ATPase motor. However, the number of possible states of F_1-ATPase was 64 and certain transitions could be *a priori* excluded as unrealistic.

The authors of the model do not consider cargo movements. For this reason, it has limited application. Nor does it take account of noises produced by fluctuations of hydrolysis time.

5.2 Dynein with struts ('crutches')

The method proposed in Section 5.1 can be extended to calculate the motion of dynein with struts. The hypothetical structure of such a motor was presented in Ref. [44] (Fig. 21).

Dynein motors do not efficiently walk along microtubules unless they are in a tripartite complex with an adapter molecule, e.g., BicD2, and dinactin facilitating dynein motion. These complexes have 'crutches' also connected to microtubules, while the adapter is also attached to the cargo transported [44]. Such a structure efficiently operates in cells by contributing to collective generation of forces for mitotic events.

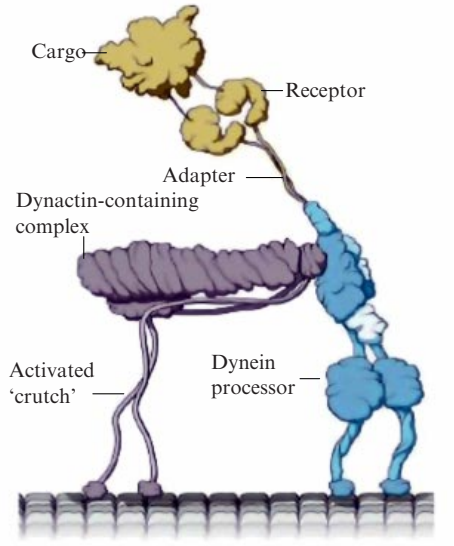

Figure 21. (Color online.) Hypothetical structure of dynein with 'struts' (taken from Ref. [44]).

Such a dynein with 'crutches' is believed to perform a rectilinear motion along an MT without the leg hopping from one microtubule to the other. We think that such stepping behavior can be described by a dynamic model like that proposed in Ref. [45]. This mathematical model is built around a system of dynamic equations into which the following desired functions were introduced: coordinates of the two 'feet' in contact with the MT, coordinates of the centers of masses of two drivers with ATPase centers of AAA1 exerting initial forces, and coordinates of the cargo attached to the tails. Angles are introduced between the 'leg' direction and horizontal direction in which the centers of drivers move, and between tail directrixes and the direction of motion of the drivers' centers of masses. The model lacks fluctuation variables but permits monitoring the stepping dynamics. Also, it readily allows variables describing 'crutch' stepping and random actions.

5.3 Rayleigh equations for molecular motors exemplified by kinesin

All MM models considered in the preceding sections can be reduced to systems of generalized Rayleigh equations. Moreover, it was shown in Ref. [46] that models describing the dynamics of oscillatory processes in biophysics can also be reduced to such systems, including the FitzHugh–Nagumo type equations, Sel'kov's model of self-oscillations in glycolysis, and the well-known Brusselator equation. Let us discuss this issue with reference to kinesin. Eliminating elastic strain τ from system (4) yields the generalized Rayleigh equation for each 'leg'. Then, the dynamic system for the whole MM can be reduced to the following form:

$$\varsigma\,\frac{\mathrm{d}^2\beta_1}{\mathrm{d}t^2} - (1 - \varsigma - \beta_1^{n-1})\,\frac{\mathrm{d}\beta_1}{\mathrm{d}t} + \left[(k-1) + \frac{\beta_1^{n-1}}{n}\right]\beta_1 + \varepsilon k\left(\frac{\mathrm{d}\beta_2}{\mathrm{d}t} - \frac{\mathrm{d}\beta_1}{\mathrm{d}t}\right) = 0\,,$$

$$\varsigma\,\frac{\mathrm{d}^2\beta_2}{\mathrm{d}t^2} - (1 - \varsigma - \beta_2^{n-1})\,\frac{\mathrm{d}\beta_2}{\mathrm{d}t} + \left[(k-1) + \frac{\beta_2^{n-1}}{n}\right]\beta_2 + \varepsilon k\left(\frac{\mathrm{d}\beta_1}{\mathrm{d}t} - \frac{\mathrm{d}\beta_2}{\mathrm{d}t}\right) = 0\,. \tag{14}$$

Here, the tilde symbol in notations of variables and parameters is removed, the torque exerted by pulling out the 'foot' of the rear (second) 'leg' by the front (first) 'leg' is supposed to be small and proportional to $\mathrm{d}\beta_1/\mathrm{d}t$ (and vice versa). Also, the smallness of parameter ε with respect to other coefficients of this system is taken into account. When considering the sequence of steps, coefficients ς and ε must change values depending on the sign of $\mathrm{d}\beta_i/\mathrm{d}t$ for the ith equation ($i = 1, 2$).

Figure 22 presents an example of a solution for system (14).[4]

Figure 22c–e shows 35-ms substeps within a step of kinesin traveling along the MT axis. The ATP level in the medium is assumed to be high; therefore, stepping occurs

[4] Calculations made by A V Kargovsky.

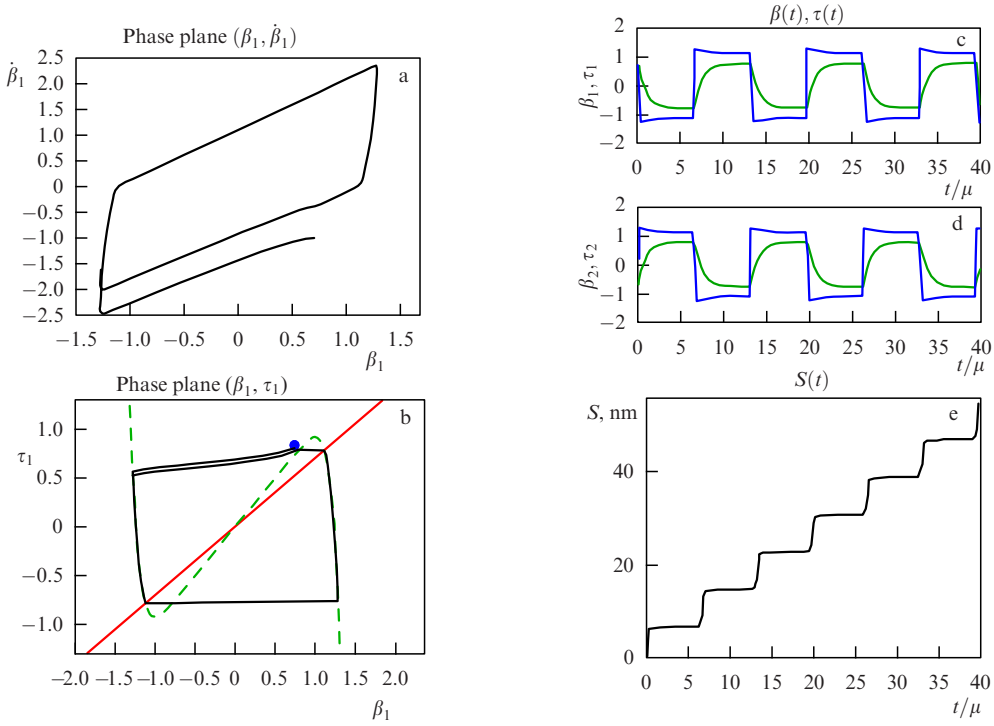

Figure 22. Phase planes $(\beta_1, \dot{\beta}_1)$ (a), and (β_1, τ_1) (b). Solutions of system (14) for $\beta_1(t)$, $\tau_1(t)$ (c), and $\beta_2(t)$, $\tau_2(t)$ (d). Displacement of the center of mass along the MT axis (e). Parameters of the model: $n = 13$, $\varsigma = 0.1$, $\varepsilon = 0.04$, $k = 0.7$, and $\mu = 5$ ms.

without accidental delays on the timescale. The length of the substeps is close to its minimal value in experimental stepping records (see Fig. 5).

Each of the equations in system (14) must take account of accidental dwell times for ATP sorption in ACs, when its level in the medium is low. Moreover, the equations must include thermal noises, multiplicative noises arising from fluctuations of ATP hydrolysis time in ACs, and times of product release from ACs. Meeting these conditions for noise is essential for addressing the problem of the effectiveness of cargo dragging over by MMs (see Ref. [47]).

6. Discussion. Unresolved problems

To begin with, a wide variety of unsolved problems are directly related to the competence of researchers, their ability to cope with them, and the range of literature publications available.

6.1 Microtubule network — a molecular substrate for neuronal transport [5]

The neuronal transport system is based on the microtubule network. MTs grow continuously after the appearance of the new dendrites and regenerate when necessary. This process consumes energy and is certainly supported by GTPases functioning as a sort of MMs (guanosine triphosphate or GTP is an analog of ATP synthesized using it as the phosphate donor). The microtubule network in neurons and all other cells perform a number of key functions (in mitosis, etc.). Its extreme rigidity greatly contributes to the formation of cell structure, while the AF network determines the properties of the perimembrane layer.

[5] This section was written jointly with N B Gudimchuk, a co-author of Ref. [48].

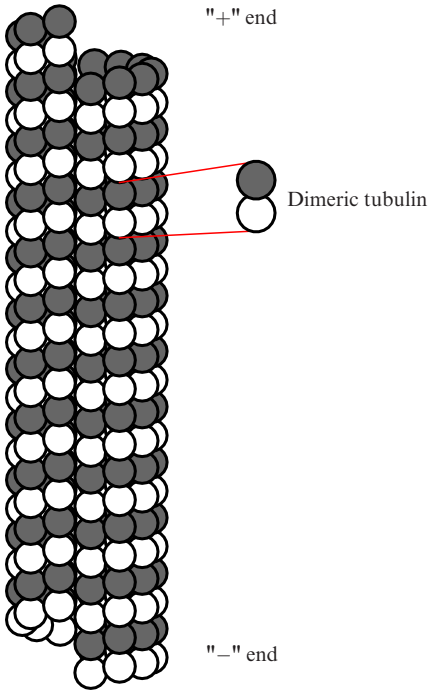

Figure 23. Schematic representation of a microtubule composed of 13 protofilaments forming a cylinder. Each β-monomer of tubulin is shown as a grey ball, and each α-monomer as a white ball.

General information about MTs can be found in Ref. [47] and references cited therein. MTs are linear polymers built up from dimeric tubulin protein (Fig. 23). The tubulin dimers make up 13 chains or protofilaments. Each protofilament is bound on both sides to two others, and the resulting structure is shaped like a cylinder 25 nm in diameter.

A MM grows as tubulin dimers attach to its end. Each tubulin monomer in an attached dimer is bound to a GTP molecule. Soon after attachment of tubulin to the MM, the β-monomer-bound GTP undergoes hydrolysis. This means that it loses phosphate and the molecule is converted into guanosine diphosphate (GDP). GTP hydrolysis inside a tubulin dimer causes a conformational change apparent, first, as its bending and, second, as its turn relative to the underlying dimer in the same protofilament. Taken together, these changes result in a protofilament composed of GDP dimers tending to bend into a horn with a radius of curvature of around 20 nm, whereas the protofilament consisting of GTP dimers of tubulin make up a straight linear structure. As the attachment of GTP dimers from the solution to the MT end continues and is followed by their hydrolysis, the MT lengthens and retains on its end dimers containing an intact GTP molecule. Because GTP dimers tend to straighten at the growing MT end, this layer encircling the MT does not permit the underlying GDP dimers to bend outwards and thereby prevents MT destruction. This layer of GTP dimers at the end of the growing MT is termed the 'cap'.

Anyway, GTP entering the gap between tubulin dimers causes their deformation.Then, it is hydrolyzed into phosphate, leaving the gap, and GDP remaining bound to tubulin β-monomer. In other words, we are dealing with a 'disposable' GTPase MM. In the absence of the cap's protective effect, filaments of tubulin dimers bend and generate a force that can be applied, for example, to proteins of the kinetochore complex having a circular structure in yeasts and a fibrillar one in animals. It enables MTs to drag over chromosomes during mitosis [16, 49, 50].

MT growth rate and GTP consumption per unit length

Here is brief quantitative information about MT growth. Let a rather long MT be further lengthened by 1 μm. How many GTP molecules need to be hydrolized? The number of tubulin layers per micrometer amounts to 1000 nm/8 nm = 125. The number of tubulin dimers in 125 layers is $125 \times 13 = 1626$. According to Ref. [51], the MT growth rate reaches 0.22 μm s^{-1}, which means that the MT lengthens by 1 μm for 4.5 s and spends 1625 GTP molecules. Thus, the rate of GTP consumption at the MT growth reaches 357 molecules per second. These data allow the consumption of GTP by the MT to be evaluated, although it is difficult to evaluate the hydrolysis rate constants and the rate of reaction product release from AC, because hydrolysis is a delayed process and occurs only some time after GTP-tubulins are built into MTs. New GTP-tubulins can join before the underlying ones undergo hydrolysis. Different authors estimate the hydrolysis rate constant at 0.04–0.3 events per second.

However, it is all much more interesting. Recent experiments have demonstrated that the MT growth rate varies periodically even if tubulin concentration in the medium remains constant. Various models of this phenomenon are considered in review [48]. The most plausible of them are constructed by the molecular dynamics method using ultrafast computers. Of special importance is a small region at the growing end of an MT, the so-called cap. Some way or another, MT growth is a self-oscillatory and even autowave process. It is therefore clear that the superposition of an external chemical wave may cause modulation of the MM stepping rate on MTs (see below).

Models for regulation of MT operational efficiency (*conducting capacity*)

Mathematical models describing effects of various biochemical factors on traffic block (i.e., inhibition of MM stepping along an MT) have been extensively elaborated in recent years. Specifically, the action of AC binding inhibitors on MTs leading to the most serious consequences for the organism is being investigated [52]. AC binding inhibition by modified tau-protein is especially attracting much attention, since tau-acetylation in patients exhibiting Alzheimer's disease and other neurodegenerative conditions disturbs one of the most important functions of tau-proteins, i.e., regulation of MT assembly, and contributes to pathological aggregation. One recent publication proposes a mathematical model for regulation of MM flow density and rate on MTs in long axons. The authors argue that such regulation is facilitated by the waves of chemically active stimulators excited along the axons [53].

Reference [54] reports new experimental data on *in vitro* MT growth in the presence of various chemical factors stimulating or inhibiting it. Moreover, the authors describe in quantitative terms the development of MT networks depending on the angles at which microtubules adjoin each other in the presence of stepping kinesins. These results may provide a basis for the construction of distributed mathematical models predicting the effects of various toxins and pharmaceutical products.

The above brief overview of MTs may be used to write an article concerning a mathematical model of MT growth and conductivity regulation.

6.2 Problems of neuron energetics

Many processes in the neuron, including the maintenance of stationary membrane potential, are driven by the MM pump of Na^+, K^+-ATPase. In addition, energy is consumed to support the work of the genetic apparatus, synthesis of necessary enzymes, upkeep of the mitochondrial structure, and repair of the transport system.

Transport expenses account for about 5% of a neuron's total energy expenditure, equivalent to $\sim 10^{10}$ ATP molecules per second, i.e., $\sim 10^8$/s. To recall, the number of ATP molecules consumed by large and branched axons is much greater than for an 'averaged' neuron.

How much ATP is spent to ensure kinesin walk along a squid axon? The axon is 1 m long and one kinesin step is 8 nm, which means that kinesin would have to take 10^8 steps using 10^8 ATP molecules for ~ 50 ms $\times 10^8 \approx 5 \times 10^6$ s or roughly 5 days!! In other words, the work of several kinesins is needed to drag over a single mitochondrion from the nucleus to a synapse.

MM transport declines when mitochondria and other vesicles accumulate in the synaptic terminal, as was demonstrated for the Neurospora transport system [55], where the delivered cargo is used for invagination synthesis and the growth of the cell's terminal regions.

It is not at all necessary to transport a damaged mitochondrion from the synaptic terminal to the nucleus, because intermediate synthesis may just as well occur in the depot where it eventually finds itself. Ingredients for its repair appear to enter the depot from myelin-producing cells arrayed along the entire length of the axon. The propagation speed of the nerve impulse and the respective synaptic excitation are unrelated to the MM stepping rate provided the synaptic terminal contains enough vesicles with neuromediators.

Human motoneurons are very long too, but they are surrounded by insulating myelin-forming cells. An impulse

propagates in them from one 'relay station' to another with negligible losses. The relays (Ranvier's constrictions) are spaced a few micrometers apart. But both kinesin and dynein have to walk over such long motoneurons. In all probability, they do not always start or finish near the nucleus. There is evidence that the enzyme synthesizing acetylcholine from acetate and choline penetrates into neuroplasm (depot) from myelin-producing cells. The problem of neuron energetics, including the role of Ranvier's constrictions and possible spontaneous generation of nerve impulses under the effect of fluctuations, is considered in Ref. [56]. In conclusion, it is opportune to say that the work of MMs cannot be understood without reference to fluctuations of one sort or another.

6.3 Role of noises in the work of molecular motors

It was shown in the foregoing that any MM step depends on random sorption of ATP in the AC. ATP penetration into the AC was studied by G Oster Lab [14]. Analyzing this problem would allow us to understand how the sorption forces get involved as ATP enters the AC. In all likelihood, this process occurs predominantly via sequential formation of hydrogen bonds.

The breakage of the ATP macroergic bond during hydrolysis is a random process as well. Strictly speaking, it should be studied by quantum mechanics and molecular dynamics methods. The latter can also be applied to determine the time of release of hydrolysis products (ADP and P^-) from the AC pocket. This so far unresolved problem reduces to distinguishing between simultaneous and successive breaking of hydrogen bonds that hold the reaction products inside the AC. Therefore, coefficient μ has to be determined based on experimental data.

We did not directly take into account thermal noises in the models considered in the preceding sections, although it should have been done for the sake of completeness. Reference [47] poses the problem of evaluating the efficiency of MM operation, which is impossible to address without due regard for thermal noises and the size and shape of the cargo. Moreover, the Stokes force during stepping speed acceleration must be written bearing in mind this requirement.

6.4 Refinement of parameters responsible for the coupling of two drivers in molecular motors

One more issue remains unclear. Parameters determining the binding of motor 'legs' to an MT or AF in MM models are poorly known. It was mentioned in the foregoing text that reliable X-ray images of the 'feet' bound to the 'rails' are still lacking. The same is true of the binding of the myosin V 'mouth' to AF. Interaction among kinesin 'feet' is schematically presented in Ref. [29].

MM stepping is comprehensively and vividly (animated movies are available) represented on websites [12, 13]. The stepping pattern of a kinesin 'foot' detached from the MT is traced in paper [31]. The mathematical model of dynein with 'crutches' awaits elaboration.

There is little doubt that both coefficient K and the elastic force τ itself must be thoroughly calculated by the molecular dynamics method as described, for instance, in Ref. [40]. The $\tau(\beta)$ dependence is nonlinear in MM models. Hence, the necessity of refining their phase plane picture as reported for F_1-ATPase models in Ref. [32]. This approach made it possible to describe the two-step regime of AC packet closure. Importantly, coefficient μ in Eqns (3) must have different values for the stages of breaking up the macroergic ATP bond and liberation of hydrolysis products from the open AC pocket.

6.5 Collective dynamics of molecular motors

Another important issue is how collective and synchronous stepping of several MMs is organized when they drag over one large cargo [57, 58].

MMs operate not only in neurons but also in any other cell. Recently, much attention has been given to the organization of a kinesin network (see Fazly Ataullakhanov's website [16] and [58]).

Moreover, there is the problem of organization of myosin V and other MM networks [59] in ameboid cells (see, for instance, Refs [60, 61]. The question is how a stochastic actomysin network evolved into murine sarcomers, how calcium ions came to be regulators, and how dynein structures developed the ability to jointly operate in flagella.

The role of certain ACs in the disks of dynein motors remains obscure. An analogy suggests itself between the structures of a dynein disk and F_1-ATPase motor, also consisting of six segments.

It is important to establish a clear understanding of the relationship between models of individual MMs and the motion of active particles in a tilted periodic potential as considered in detail in Refs [62–65].

Finally, a deeper insight into the synthesis (fabrication) of MMs and their lifetime is needed. The problem of mitochondrion lifetime also refers to the same range of issues.

7. Conclusions

7.1 Unified principles behind the organization of molecular motors

Functional schemes and mathematical models of most neuronal MMs (F_0F_1-ATPase, kinesin, myosin V, dynein) are based on the same principle, viz. all these MMs consist of three or two coupled drivers [4, 66–68], each having an AC with the pocket between two subglobules joined together via a 'hinge joint'.

As an ATP molecule penetrates into the AC of one of the drivers, the pocket deforms under the effect of sorption forces. The strain can be roughly described by a decrease in the angle between the subglobules. In its turn, the motion of subglobules in one AC exerts a torque that causes, via the kinematic connection, the rotor in F_1-ATPase or the cargo-moving 'neck' in the kinesin to rotate. In addition, a smaller torque is generated that starts up the second motor tied up with the first one, activates F_1-ATPase, or 'pulls out' the rear leg.

In the case of myosin V or dynein, the torque of sorption forces first induces elastic strain proportional to a decrease in the angle between subglobules in the motor unconnected to an AF or MT. Only after the leg of this motor comes into contact with either AF or MT, the energy stored in elastic strain is utilized to generate a torque needed to drag over the cargo.

The mechanisms of F_1-ATPase, kinesin, and myosin V action are known fairly well, whereas the intricate structure of the dynein motor remains to be elucidated. In particular, the role of all six ACs of its 'drum' is still unclear. In addition to neurons, myosin motors are 'collectively' employed in muscle cell sarcomers [6], and dynein motors in the flagella and cilia of plants and animals [69, 70]. In this context, it is important

to understand how the models of individual MMs proposed thus far can be used to simulate their associations.

Also noteworthy is the crucial role played in neurons by such MMs as Na^+, K^+-ATPase (pump) and GTPase motor contributing to MM building (lengthening). The structure of their mathematical models remains to be elaborated. There is little doubt that they should include sorption forces arising when ATP or GTP penetrate an AC. Neuronal transport in the vegetative nervous system deserves special consideration in order to differentiate between MMs operating in neurons and other living cells, e.g. yeasts.

7.2 Problems of neuron and brain energetics

Neuronal energetics or energy consumption was considered in Section 1.3 of the Introduction with reference to the most common types of neurons and synapses in the central nervous system (see also Section 6.2).

However, there are many kinds of neurons substantially differing from one another in terms of size, structure, and function, e.g., very large cortical pyramidal neurons up to 100 μm in diameter with long myelinated processes and tiny interneurons (~ 4 μm in diameter). The modes of operation of neurons are different, too; they vary from the generation of single action potentials with a mean frequency not higher than a few impulses per second to producing packets of action potentials (the so-called pacemaker regime in which a neuron generates hundreds of impulses per second over a long time span). A special review is needed to comprehensively describe the energetics of particular types of neurons.

Another important issue is whole brain energetics. What are the energy requirements of the neurons transmitting impulses from the sense organs? (By way of example, neurons processing auditory information must be able to generate action potentials with a frequency up to 1000 impulses/s and an accuracy up to a few μs.) What are the brain energetics during sleep? What is the total energy consumed by the brain depending on the 'value' of new information it receives? How much energy is spent by different brain regions and neurons in someone making calculations? And how much energy is needed to preserve the memory of an image, e.g., A A Ivanov's picture *The Appearance of Christ Before the People*, for 10 years? These and related issues are extensively being explored by researchers dealing with neural networks. The question is, what are the energetics of these processes?

Acknowledgments

When working on this review, we had the pleasure to collaborate with A R Brazhe, N G Gudimchuk, and A V Kargovsky. The helpful discussions with N A Kubasova, N K Lavrova, A V Latanov, Ya R Nartsissov, E B Postnikov, G Yu Riznichenko, V A Teplov, A N Tikhonov, A K Tsaturyan, and D S Chernavsky are greatly appreciated. Also to be thanked are our German colleagues L Schimansky-Geier and W Ebeling.

Such an extensive list of our colleagues is presented here to facilitate searching for information for those interested in the issues touched upon in this review.

The work was partly supported by RFBR grant No. 13-02-01177A and delivered at a plenary session of the Fifth Congress of Russian Biophysicists (Rostov-on-Don, October 2015).

Appendix. List of abbreviations

ADP — adenosine-5′-diphosphoric acid
ATP — adenosine-5′-triphosphoric acid
AF — actin filament
ACh — acetylcholine
AChE — acetylcholinesterase
AC — active center
KH — kinesin head
MM — molecular motor
MT — tubulin microtubule

References

1. Ivanitskii G R, in *V S'ezd Biofizikov Rossii, 4–10 Oktyabrya 2015 g. Materialy* (V Congress of Russian Biophysicists, 4–10 October 2015. Abstracts) Vol. 1 (Rostov-on-Don: Izd. Yuzhnogo Federal'nogo Univ., 2015) p. 26
2. Romanovsky Yu M, Tikhonov A N *Phys. Usp.* **53** 893 (2010); *Usp. Fiz. Nauk* **180** 931 (2010)
3. Chernavsky D S, Khurgin Yu I, Shnol' S E *Mol. Biol.* **1** 419 (1967)
4. Chernavsky D S, Chernavskaya N M *Belok-Mashina. Biologicheskie i Makromolekulyarnye Konstruktsii* (The Protein Machine. Biological and Macromolecular Structures) (Moscow: Yanus-K, 1999)
5. Eide J L, Chakraborty A K, Oster G F *Biophys. J.* **90** 4281 (2006)
6. Kubasova N A, Tsaturyan A K *Usp. Biol. Khim.* **51** 233 (2011)
7. Roberts A J et al. *Nature Rev. Mol. Cell Biol.* **14** 713 (2013)
8. Vale R D et al. *Cell* **40** 449 (1985)
9. Schnapp B J et al. *Cell* **40** 455 (1985)
10. Squire L et al. (Eds) *Fundamental Neuroscience* 3rd ed. (San Diego: Academic Press, 2008)
11. Latanov A V *Obshchaya Neirofiziologiya. Kurs Lektsii* (General Neurophysiology: The Course of Lectures) (Moscow: Izd. MGU, 2013)
12. R.D. Vale Lab, http://valelab.ucsf.edu/
13. S.M. Block Lab, https://blocklab.stanford.edu/
14. G Oster Lab, http://www.cnr.berkeley.edu/~goster/home.html
15. Leslie A G W, Walker J E *Phil. Trans. R. Soc. Lond. B* **355** 465 (2000); J. Walker Lab, https://walker.biology.missouri.edu/
16. Hematological Research Centre, Russian Ministry of Health. Laboratory of Physical Biochemistry, http://fazly.ru/index.php/ru
17. Rubin A B *Biofizika* (Biophysics) (Moscow–Izhevsk: Inst. Komp'yut. Issled., 2013) in 3 volumes
18. Murray J D *Mathematical Biology* Vol. 1 *An Introduction* (New York: Springer, 2002); Translated into Russian: *Matematicheskaya Biologiya* Vol. 1 *Vvedenie* (Moscow–Izhevsk: Inst. Komp'yut. Issled., 2009)
19. Howarth C, Gleeson P, Attwell D *J. Cereb. Blood Flow Metab.* **32** 1222 (2012)
20. Sokoloff L et al. *J. Neurochem.* **28** 897 (1977)
21. Jain KK, Fischer B, in *Oxygen in Physiology and Medicine* (Eds K K Jain, B Fischer) (Springfield, IL: Charles C. Thomas, 1989) pp. 25 – 53
22. Ebeling W, Schimansky-Geier L, Romanovsky Yu M (Eds) *Stochastic Dynamics of Reacting Biomolecules* (River Edge, N.J.: World Scientific, 2002)
23. Chikishev A Yu, Kroo S V, Netrebko A V, Netrebko N V, Romanovsky Yu, in *Stochastic Dynamics of Reacting Biomolecules* (Eds W Ebeling, L Schimansky-Geier, Yu M Romanovsky) (River Edge, N.J.: World Scientific, 2002) pp. 206 – 246
24. Chikishev A Yu, Grishanin B A, Shuvalova E V, in *Stochastic Dynamics of Reacting Biomolecules* (Eds W Ebeling, L Schimansky-Geier, Yu M Romanovsky) (River Edge, N.J.: World Scientific, 2002) pp. 247 – 262
25. Sussman J et al. *Science* **253** 872 (1991)
26. Reck-Peterson S L, Vale R D, Gennerich A, in *Handbook of Dynein* (Eds K Hirose, L Amos) (Boca Raton, FL: Pan Stanford Publ., 2012) pp. 145 – 171
27. Trybus K M *Cell Mol. Life Sci.* **65** 1378 (2008)
28. Schnitzer M J, Visscher K, Block S M *Nature Cell Biol.* **2** 718 (2000)
29. Asbury C L, Fehr A N, Block S M *Science* **302** 2130 (2003)

30. Sindelar C V, Downing K H *Proc. Natl. Acad. Sci. USA* **107** 4111 (2010)
31. Hwang W, Lang M J, Karplus M *Structure* **16** 62 (2008)
32. Kargovsky A V, Romanovsky Yu M, Tikhonov A N *Biophysics* **54** 1 (2009); *Biofizika* **54** 5 (2009)
33. Pogrebnaya A, Romanovsky Yu, Tikhonov A *Fluct. Noise Lett.* **5** L217 (2005)
34. Romanovsky Yu M, Kargovsky A V, Ebeling W *Eur. Phys. J. Spec. Top.* **222** 2465 (2013)
35. Xing J, Liao J-C, Oster G *Proc. Natl. Acad. Sci. USA* **102** 16539 (2005)
36. Romanovsky Yu M, Kargovsky A V, Priezzhev A V, Trifonenkov V P "Vnutrikletochnaya avtovolnovaya gidrodinamika i molekulyarnye motory" ("Intracellular autowave hydrodynamics and molecular motors"), in *Trudy XII Mezhdunarodnoi Nauchno-Tekhnicheskoi Konf. "Opticheskie Metody Issledovaniya Potokov" 25–28 Iyunya 2013* (Proc. of the XII Intern. Scientific and Technical Conf. "Optical Methods of Flow Investigation" 25–28 June 2013) (Moscow: Pero, 2013) pp. 1–21
37. Visscher K, Schnitzer M J, Block S M *Nature Lett.* **400** 184 (1999)
38. Schnitzer M J, Visscher K, Block S M *Nature Cell Biol.* **2** 718 (2000)
39. Svoboda K, Block S M *Annu. Rev. Biophys. Biomol. Struct.* **23** 247 (1994)
40. Craiga E M, Linkea H *Proc. Natl. Acad. Sci. USA* **106** 18261 (2009)
41. Kikkawa M *J. Cell Biol.* **202** (1) 15 (2013)
42. Samara L et al. *Cell* **126** 335 (2006)
43. Sarlah A, Vilfan A *Biophys. J.* **107** 662 (2014)
44. Allan V *Science* **345** 271 (2014)
45. Crossley L et al. *Bull. Math. Biol.* **74** 2032 (2012)
46. Lavrova A I, Postnikov E B, Romanovsky Yu M *Phys. Usp.* **52** 1239 (2009); *Usp. Fiz. Nauk* **179** 1327 (2009)
47. Ebeling W *Eur. Phys. J. Spec. Top.* **224** 1395 (2015)
48. Gudimchuk N G et al. *Priroda* (10) 3 (2015)
49. Westermann S et al. *Mol. Cell* **17** 277 (2005)
50. McIntosh J R et al. *Cell* **135** 322 (2008)
51. Stepanova T et al. *J. Neurosci.* **23** 2655 (2003)
52. Kuznetsova I A, Kuznetsov A V *Comput. Meth. Biomech. Biomed. Eng.* **18** 1485 (2015)
53. Karamched B R, Bressloff P K *Biophys. J.* **108** 2408 (2015)
54. Doodhi H et al. *Curr. Biol.* **24** 322 (2014)
55. Potapova T V et al. *Biol. Membrany* **28** (3) 45 (2011)
56. Brazhe A R et al. *Interface Focus* **1** 86 (2010)
57. Rai A K et al. *Cell* **152** 172 (2013)
58. Furuta K et al. *Proc. Natl. Acad. Sci. USA* **110** 501 (2013)
59. Novikov K A, Romanyukha A A, in *Trudy XII Vseros. Soveshch. po Problemam Upravleniya. VSPU-2014, Moskva 16–19 Iyunya 2014 g.* (Proc. of the XII All-Russia Meeting on Control Sciences. VSPU-2014, Moscow, 16–19 June 2014) (Moscow: Inst. of Control Sciences of the Russian Academy of Sciences, 2014) p. 6595
60. Romanovskii Yu M, Teplov V A *Phys. Usp.* **38** 521 (1995); *Usp. Fiz. Nauk* **165** 555 (1995)
61. Dembo M *Biophys. J.* **55** 1053 (1989)
62. Hänggi P, Marchesoni F *Rev. Mod. Phys.* **81** 387 (2009)
63. Romanczuk P et al. *Eur. Phys. J. Spec. Top.* **202** 1 (2012)
64. Romanczuk P et al. *Chaos* **21** 047517 (2011)
65. Hennig D et al. *Phys. Rep.* **586** 1 (2015)
66. Trifonenkov V P, Kargovsky A V *Komp'yut. Issled. Modelir.* **6** 747 (2014)
67. Kargovsky A V, Romanovsky Yu M, Trifonenkov V P, in *Materials of Intern. Symp. "Biological Motility: New Facts and Hypotheses"* (Pushchino: ITEB RAS, 2014) pp. 106 – 108
68. Kargovsky A V, Romanovsky Yu M, Trifonenkov V P, Trifonenkov A V *Lektsii po Neiroinformatike* (Lectures on Neuroinformatics) (Moscow: National Research Nuclear Univ. MEPhI, Moscow Engineering Physics Inst., 2015) pp. 156–184
69. Metelina A L *Usp. Biol. Khim.* **41** 29 (2001)
70. Roberts A J et al. *Nature Rev. Mol. Cell Biol.* **14** 713 (2013)